CRITICAL REVIEW

Check for updates

Recent advances in nanomaterial-based solid-contact ion-selective electrodes

Seyed Oveis Mirabootalebi and Yang Liu ID *

Solid-contact ion-selective electrodes (SC-ISEs) are advanced potentiometric sensors with great capability to detect a wide range of ions for the monitoring of industrial processes and environmental pollutants, as well as the determination of electrolytes for clinical analysis. Over the past decades, the innovative design of ion-selective electrodes (ISEs), specifically SC-ISEs, to improve potential stability and miniaturization for *in situ*/real-time analysis, has attracted considerable interest. Recently, the utilisation of nanomaterials was particularly prominent in SC-ISEs due to their excellent physical and chemical properties. In this article, we review the recent applications of various types of nanostructured materials that are composed of carbon, metals and polymers for the development of SC-ISEs. The challenges and opportunities in this field, along with the prospects for future applications of nanomaterials in SC-ISEs are also discussed.

Introduction

The detection of ionic compounds plays an important role in various fields including water quality monitoring and disease diagnosis. Among various types of ionic sensors, electrochemical detectors are widely used due to their simple setup, low detection limit, fast response, and high selectivity.[1–3] There are several electrochemical techniques that have been successfully applied for the development of ionic sensors, such as amperometry, voltammetry and potentiometry.[4,5] Potentiometric ISEs have been used extensively in various applications including clinical diagnosis, environmental monitoring, and industrial process control. In this method, an electrode with a membrane is designed to be selective to a specific ion, and thus the activity of the target ion is measured based on the potential difference between the inner and outer surfaces of the membrane. This approach is simple, quick, cost-effective, non-destructive, and has good selectivity and a wide linear range to test biological and environmental samples.[6–9] The main challenges of conventional liquid-contact ISEs include low stability resulting from leakage of the internal electrolyte, intensive maintenance due to electrode potential drift, and limited durability. SC-ISEs can circumvent these challenges by eliminating the liquid component; this has led to improved stability, longer lifetimes, and reduced maintenance costs. However, there is a need for improvements in the performance of SC-ISEs, specifically in terms of reproducibil-

ity, selectivity, and sensitivity. This is particularly important for analysing a wide range of real samples under non-laboratory conditions, such as *in situ* monitoring of ions in harsh environments or real-time monitoring of biological samples.

In recent years, the innovative design of ISEs by integrating advanced materials into different components such as membranes, transducers and their interfaces has attracted considerable interest to improve the performance of ISEs.[10–13] Nanomaterials are an important group of advanced materials, encompassing a wide range of structures such as nanospheres, nanotubes, nanorods, nanowires, nanofibers, nanoclusters, and quantum dots, in which at least one of their dimensions is less than 100 nm.[14] Due to ultra-high surface areas, nanomaterials show unique properties compared with bulk materials,[15] making them promising candidates for the development of the next generation of SC-ISEs. For example, nanomaterials with high conductivity, light insensitivity, and low interference by O_2 and CO_2 have better signal stability than bulk materials.

The application of nanomaterials as a component of ISEs was initiated in 1994 when Diamond *et al.*[16] predicted the development of new generations of intelligent sensing systems, with the rapid progress in nanotechnology. In 1997, Ghadiri *et al.*[17] introduced a novel diffusion-limited size-selective ion sensor based on monolayer-supported peptide nanotubes on a gold film. Nowadays, many types of nanomaterials including carbon nanotubes (CNTs), graphene, fullerene, carbon black, three-dimensionally ordered microporous (3DOM) carbon, metal and polymer nanomaterials, as well as nanocomposites have been investigated for the development of the next generation of ISEs.[18–21]

College of Science and Engineering, James Cook University, Townsville, Queensland 4811, Australia. E-mail: yang.liu11@jcu.edu.au

In recent years, although there have been several review papers published in the area of SC-ISEs, which have provided comprehensive information on mechanisms and applications of SC-ISEs,[11,22,23] none of them have focused on the evaluation, discussion, and identification of the challenges in nanomaterial-based SC-ISEs, which are of significant importance for the future development of low-cost and high-performance chemical sensors. Additionally, regarding SC-ISEs based on nanomaterials, most of these reviews focus on the use of nanomaterials as transducers of SC-ISEs. Although it is the most common way to improve the sensing performance,[11,22,23] the benefit of using nanomaterials in other parts of ISEs should not be ignored. In this review, an overview of recent advances in nanomaterial-based SC-ISEs over the last five years is provided, with an emphasis on the applications of various types of nanomaterials as different components of SC-ISEs. Furthermore, comments on the main progress and challenges, as well as the potential of using nanomaterials for the design of SC-ISEs with improved sensing performance are also provided and discussed.

ISE structures and mechanisms

Traditionally, an ISE is composed of an ion-selective membrane, reference electrodes and inner reference solution, operating based on potentiometry and following the Nernst equation. The ion-selective membrane selectively interacts with the ion of interest while excluding the other ions. The reference electrode, *e.g.*, the Ag/AgCl electrode, has a highly reproducible and stable potential and is widely used in ISEs. Given that all reference and junction potentials can be assumed to be constant, the ion-selective membrane is the central component of ISEs, governing the overall potential and ion movements.[24,25] In addition to traditional liquid-contact ISEs, SC-ISEs were developed by replacing the internal solution with a transducer that enabled ion-to-electron transduction.[26] They addressed inherent limitations of traditional ISEs associated with the use of an internal reference solution, including liquid junction potential issues, solution evaporation, electrode fouling, and limited miniaturization capacity.

The principles of ion-selective sensors are rooted in the relationship between ion activity and output voltage, as defined by the Nernst equation.[6,27] At electrochemical equilibrium of an ISE, the solution/membrane interface undergoes the formation of an electrical double layer, leading to the generation of an electrical potential difference. The following equation predicts a linear dependence of the potentiometric sensor response (E) based on a function of the ion's activity:[28]

$$E = E^{\circ} + \frac{RT}{nF}\ln[a_i] \qquad (1)$$

where R is the gas constant, F is the Faraday constant, n denotes the electron count, a_i is the activity of the primary ion, and E° is the standard potential, which is a key parameter for the reproducibility of potentiometric sensors.

Converting the ionic signal to the detectable electrical signal, which is performed through the transducer layer, plays a significant role in the potential stability, lifetime, sensitivity, response time, and reproducibility of SC-ISEs. The ion-to-electron transition mechanism in traditional liquid-contact ISEs is based on an internal reference electrode and an inner filling solution, which enable the ion transition *via* a reversible redox reaction. While this approach offers advantages such as the simplicity of the process, it encounters limitations like portability, lifetime, and fragility due to the nature of the liquid contact. In SC-ISEs, the charge transition from an ion to an electron is governed by the transducer functional material. There are two main types of SC-ISEs, requiring distinct ion-to-electron transducer materials. The transducer based on redox capacitance typically involves the use of redox polymers or other electroactive materials, such as redox couple doped gold nanostructures. The ion-to-electron procedure is like the process for the internal reference electrode of traditional ISEs as described by:

$$M^+A^- + e \rightleftarrows M + A^-$$

where M^+ is a metal ion or oxidized conductive polymer, M is a metal or neutral conductive polymer, and A^- is an anion. Conductive polymers are commonly used as the solid contact in ISEs; however, the possible formation of a water layer, as well as their sensitivity to oxygen and light are potential limitations in practical applications. On the other hand, the transducer based on double-layer capacitance utilizes materials with a large surface area. Instead of a redox process, a large double layer capacitance is created at the surface of the solid contact, and thus the interfacial potential is produced based on the number of charges in the electrical double layer. Since this mechanism depends on the large interfacial potential between the solid contact and the membrane, nanomaterials such as carbon-based nanomaterials (carbon nanotubes, graphene, and fullerene) and some metal–organic frameworks (MOFs),[11,29–32] which naturally have a high surface area, have been extensively used based on this mechanism.

Although the SC-ISEs exhibit improved performance, there are several problems to address, including potential instability and poor reproducibility. For example, dissolved O_2 and CO_2, which may reach the solid contact, can generate side reactions in parallel to the ion-to-electron transduction procedure.[33] These reactions can interfere with the electrochemical processes involved in the detection of target ions. In a similar way, exposure to light during measurements, especially in harsh environmental situations, *e.g.*, intense sunlight, can induce photochemical reactions that may interfere with the electrochemical processes, resulting in a poor response accuracy of SC-ISEs. Furthermore, a water layer formed between the membrane and the solid contact of SC-ISEs serves as an electrolyte reservoir, which equilibrates after every change in the sample's composition, leading to high limits of detection (LODs) and low potential stability.[34,35]

To overcome these challenges, different types of nanomaterials have been employed in SC-ISEs. Although nanomaterials have been employed in the components of external reference electrodes and ion-selective membranes,[36–38] most studies have concentrated on enhancing the performance of transducers with nanomaterials. Fig. 1 provides a schematic diagram of the components of a typical nanomaterial-based SC-ISE, in which nanomaterials are integrated into the transducer layer of the ISE by drop casting. The emphasis lies on improving the ion-to-electron transduction process by increasing electrical conductivity, capacitance, hydrophobicity, and surface area.

Applications of nanomaterial-based SC-ISEs

Carbon nanotubes

Among various nanomaterials, CNTs stand out as one of the most favoured materials for the development of high-performance SC-ISEs. They have tubular structures of rolled graphene sheets and are classified as single, double, and multi-walled CNTs. CNTs have various properties, such as a high surface area to volume ratio, high electrical capacitance, good hydrophobicity, high Young's modulus (≈ 1 TPa), fast charge transfer kinetics, high level of selective functionalization, and good antifouling ability, making them attractive materials for SC-ISE applications.[39–42] Therefore, CNT-based ISEs exhibit high analytical performance to detect many ions of biological and environmental importance such as K^+, Na^+, Mg^{2+}, NH_4^+, Ca^{2+}, SiO_3^{2-}, Hg^{2+}, Cd^{2+}, Pb^{2+}, NO_3^-, Al^{3+}, ClO_4^-, I^-, and Cr^{3+}.[43–53] Additionally, the CNT-based SC-ISEs were used extensively for the detection of chemical and pharmaceutical compounds such as bisphenol S,[54] fluoxetine,[55] barbital,[56] nalbuphine.[57]

Rius et al.[58] pioneered the application of CNTs in SC-ISEs by using single-walled carbon nanotubes (SWCNTs) as an ion-to-electron transducer, which exhibited good signal stability (25 days) and a short response time (fewer than 10 s for activi-

ties over $10^{-5.5}$ M) for the detection of K^+. Although it is more challenging to design SC-ISEs for the determination of anions than cations due to the smaller charge-to-radius ratio of anions, their propensity to become protonated at low pH, the influence of solvation effects, and the variability in their geometric sizes,[59] CNTs used as the inner transducer layer in SC-ISEs exhibit high capabilities for detecting both anions and cations.[60] The capacitance of the transducer layer of ISEs plays a significant role in potential stability and can also have an impact on important parameters like reproducibility and long-term performance. Zdrachek and Bakker[61] reported that the double-layer capacitance increased linearly by increasing the number of deposited CNT-based transducer layers, which led to a reduced potential drift. This method could also serve as a new way to estimate the double-layer capacitance of the SWCNT layer in the deposition process.

Serving as a reference electrode is another application of CNTs in SC-ISEs. The most commonly used reference electrode, the Ag/AgCl electrode, is not very appropriate for sweat analysis, as the potential of the electrode is highly affected by the concentration of chloride ions. Toor et al.[62] embedded a layer of CNTs between the membrane and Ag/AgCl layer to adsorb and retain chloride ions for the detection of Na^+, NH_4^+, and lactate in sweat. This method resulted in a reproducible and stable reference electrode that exhibited a negligible potential fluctuation up to 0.08 mV in a solution with chloride concentrations varying between 0.1 and 100 mM, while practical applications such as real-time monitoring of sweat on skin are expected to be investigated, considering the common issues of reproducibility and long-term stability associated with interference from the electrolytes in sweat. Hanein et al.[63] developed a wearable CNT-based SC-ISE for Na^+ detection by using CNT electrode arrays in both the solid contact and reference electrode. CNT electrodes were prepared by the synthesis of CNTs via chemical vapor deposition (CVD) on SiO_2/Si substrates. Subsequently, reference electrodes were prepared by coating the CNT electrodes with a colloidal dispersion of Ag/AgCl, agarose, NaCl, and polyvinyl chloride (PVC). The CNT-based reference electrodes showed high repeatability and low sensitivity (-1.7 ± 1.2 mV per decade) in the NaCl solution. Despite the fact that some important characterization studies including potential drift were not provided, this paper was pioneering in the application of CNTs in wearable potentiometric sensors and opened a new avenue for subsequent studies.

Carbon paste is an attractive type of electrode due to its good reusability, simple and versatile preparation procedure, and low cost.[64,65] It is generally composed of a wide range of carbon materials, additives and solvents[66] and has been used in ISEs for several decades.[67] In recent years, nanocarbon-based paste, particularly CNT paste, has been introduced into ISEs, which have exhibited improved performance for ion sensing.[68–71] For example, Ramezani and co-workers[72] developed multi-walled carbon nanotube (MWCNT)-grafted 2,6-bis[2-(amino methyl)phenol]pyridine (BAPP) synthetic ligands as novel ion carriers and signal boosters in carbon paste for the simultaneous detection of Hg^{2+} and Cu^{2+}. The modified ISE
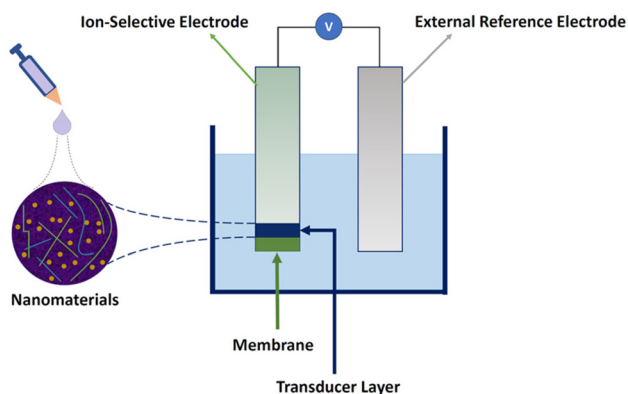

Fig. 1 A schematic representation of a typical nanomaterial-based SC-ISE.

displayed satisfactory reproducibility, with LODs of 2.0×10^{-9} and 7.9×10^{-10} mol L^{-1} for Hg^{2+} and Cu^{2+}, respectively.

Graphene

Graphene with sp^2-bonded carbon atoms has a single layer of hexagonal honeycomb structure and is known for its excellent electrical, mechanical, and thermal properties.[73,74] It is one of the most widely used carbon nanomaterials in potentiometric ISEs, which exhibit excellent analytical performances to monitor a wide range of ions such as K^+, Na^+, Pb^{2+}, Li^+, H^+, Mg^{2+}, Zn^{2+}, Ca^{2+}, and Cu^{2+}.[75–83] For the first time, Ying et al.[84] introduced a novel SC-ISE for the detection of K^+ by using graphene as the solid contact. The Nernstian response was 58.4 mV per decade in a linear range from $10^{-5.8}$ to 10^{-1} M of K^+ with a low detection limit of $10^{-6.2}$ M. The attractive feature of the graphene-based transducer in an SC-ISE is its high hydrophobicity, which prevents the formation of a water layer, thereby minimizing interference from other ions. Furthermore, it is insensitive to O_2 and CO_2, meaning that it prevents side reactions and interference with the membrane, providing more accurate analysis.

Wu and co-workers[85] proposed an SC-ISE using electrochemically reduced graphene oxide as the ion-to-electron transducer for Ca^{2+} detection, which exhibited a Nernstian slope of 29.1 mV per decade and a fast response time of less than 10 s. Moreover, a low detection limit of $10^{-5.8}$ M and high hydrophobicity were obtained. Additionally, the effects of defects in graphene on capacitance and hydrophobicity were investigated by Gan et al.[86] Fig. 2 illustrates the use of defective or high-quality graphene as the solid contact in an SC-ISE. The photograph of the contact angle test for reduced graphene oxide shows a contact angle ($\theta = 113°$) after 3 hours of reduction at 160 °C. It was found that there was a negative correlation between the hydrophobicity of graphene and its capacitance. Notably, reduced graphene oxide with a moderate level of defects demonstrated the highest potential stability by achieving a balance between hydrophobicity and capacitance.
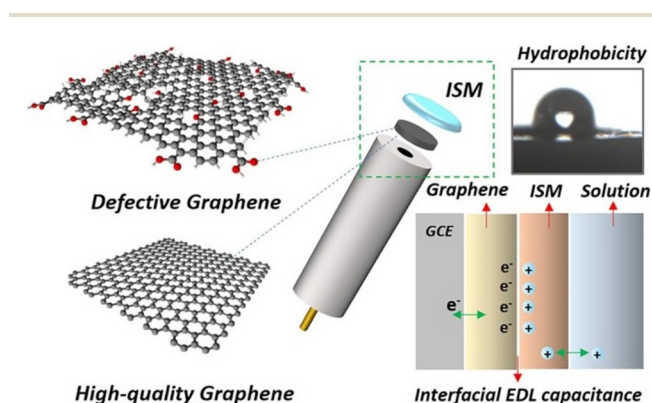

Fig. 2 Graphical summary of defective and high-quality graphene used as the solid contact material in an ISE, along with a photograph of the contact angle of water on reduced graphene oxide, and a schematic figure of the interfacial EDL capacitance of ISE.[86] Copyright 2021, Elsevier.

Recently, a new method based on laser-induced graphene was proposed for the preparation of SC-ISEs for NO_2^- detection.[87] These sensors exhibited a broad linear sensing range with high potential stability without the formation of the water layer due to the hydrophobic characteristics of the electrode. The outstanding properties can be attributed to the double-laser treatment of the graphene surface, resulting in facile electron transfer kinetics, high surface porosity, and superior conductivity.[88,89] Additionally, Gomes and co-workers[90] employed a double-laser process to produce hydrophobic laser-induced graphene, which was coated with an ion-selective membrane to form an SC-ISE for the detection of NO_3^-. The proposed ISE exhibited a low LOD (6.01 ± 1.44 μM), and the performance remained almost stable over a period of 5 weeks. The application of different types of graphene and CNTs as a transducer layer in SC-ISEs is well developed for a wide range of target analytes. However, their high costs and tedious preparation procedures become barriers in the further advancement of these SC-ISEs. Therefore, cost-effective carbon-based nanomaterials with similar physical and chemical properties to those of graphene and CNTs were investigated to circumvent these limitations.

Other nanocarbons

3DOM carbon or other forms of nanoporous carbon consist of a large amount of pores providing a high surface area and capacitance, which lead to long-term stability in the design of SC-ISEs.[91] As a solid contact, 3DOM carbon has demonstrated strong capabilities in ISEs due to its high electroactive surface area.[92–94] Bühlmann and Stein et al.[95] pioneered the investigation of 3DOM carbon in ISEs by using well-ordered interconnected macro-porous carbon as the solid contact. The generated intermediate layer stabilized the potential difference between the metallic conductor and polymer-based ion-selective membrane for K^+ detection. Su and Liu et al.[92] developed K^+ ISEs using spherical mesoporous carbon as a solid contact, resulting in an extended linear range ($10^{-4.19}$–$10^{-0.21}$ M), low LOD (5.4 μM), and a stable Nernstian response, which could be attributed to its uniform spherical structure with a mesoporous network, high capacitance, and good conductivity. Three steps were required for the preparation of ordered mesoporous carbon spheres, which made the preparation process tedious, while the high potential stability with a potential drift of 3.33 ± 0.58 μV s^{-1} showed a notable advancement in the development of potentiometric sensors. Zhong and Niu et al.[96] compared the performance of nitrogen-doped mesoporous carbon (NMC) with that of reduced graphene oxide (RGO) and CNTs for the preparation of Ca^{2+} SC-ISEs. Fig. 3A and 4B shows a scheme of the SC-ISE structure and SEM images of the three carbon nanomaterials, respectively. The chronopotentiometric results indicate that the NMC-based SC-ISE exhibited the highest capacitance (Fig. 3C), which made it advantageous for the detection of Ca^{2+} in mineral water and soil leaching solutions.[96]

Nanostructured carbon black is a cost-effective nanomaterial that can be obtained through straightforward manu-
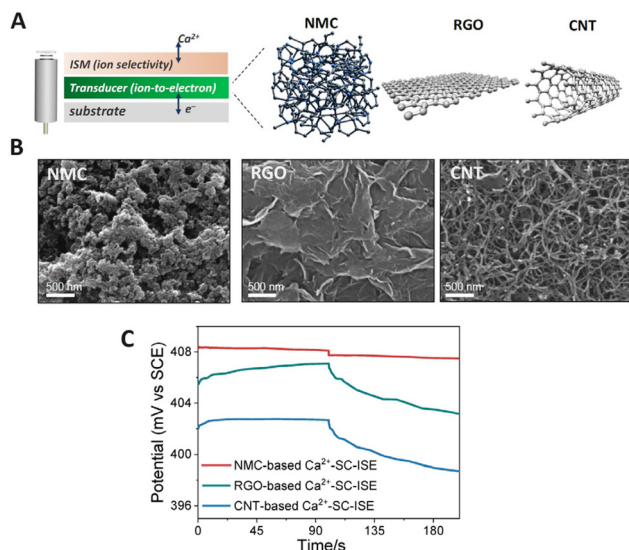
Fig. 3 (A) Schematic diagram of SC-ISEs based on NMC, RGO, and CNTs. (B) SEM images of NMC, RGO, and CNTs. (C) Chronopotentiometric curves obtained for the NMC-based, RGO-based, and CNT-based SC-ISEs for the detection of Ca^{2+}.[96] Copyright 2022, MDPI.
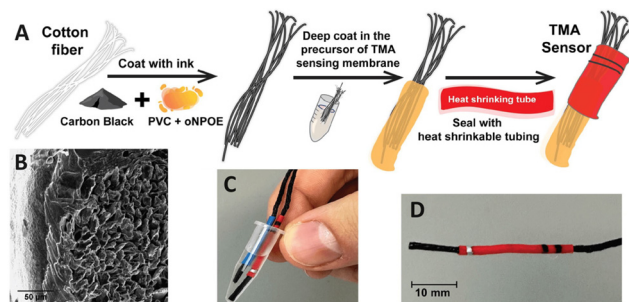

Fig. 4 (A) The process of preparing a home-made TMA sensor for vaginosis analysis. (B) A SEM cross-section image of the membrane coated TMA sensor (scale bar is 50 μm). (C and D) Photographs of the sensor depicting its portability and size.[102] Copyright 2023, MDPI.

facturing approaches and further modified to increase its surface area.[97,98] It has been successfully employed as a solid contact in ISEs due to its high porosity, good conductivity, hydrophobicity, and inert nature. Paczosa-Bator first developed an SC-ISE based on carbon black for determining K^+.[99] In a recent study, Michalska et al.[100] introduced a simple method to prepare a 3D-drawn substrate using a 3D pen containing carbon black/polymer for the preparation of disposable ISEs. This process enables electrodes to be made with desirable shapes and high device-to-device reproducibility. Moreover, carbon black has been explored to produce paste electrodes for ISE applications. Paczosa-Bator et al.[101] recently proposed a paste electrode consisting of carbon black, ruthenium, iridium, and poly(3-octylthiophene-2,5-diyl) to monitor NO_3^- in soil. The obtained results were close to the Nernst equation and showed a negligible response to interfering ions such as

Cl^-, CH_3COO^-, SO_4^{2-}, and HPO_4^{2-}, making this method suitable for analysing real samples. Furthermore, Mousavi and co-workers[102] developed a home-made SC-ISE for the rapid detection of trimethylamine (TMA) using a carbon black cotton string and a TMA selective membrane, which could be applied for the clinical diagnosis of bacterial vaginosis. Fig. 4 shows the main steps for preparing the TMA sensor, its morphological image, as well as photos of the portable sensing device. Carbon black has also been used as a solid contact in SC-ISEs for the determination of Na^+, K^+, NO_3^-, and acetylcholine,[103–108] exhibiting a Nernstian response with low LODs.

Additionally, hollow carbon nanospheres were used as the solid contact to significantly enhance the ion-to-electron transduction between the conductive substrate and the ion-selective membrane for the monitoring of Ca^{2+}.[109] The hydrophobicity, high surface area, and unique hollow structure of carbon nanospheres as a solid contact are the main reasons for the enhancement of ion-to-electron transduction. Carbon nanohorns,[110] carbon nanofibers,[111,112] and graphdiyne oxide[113] were also employed as the ion-to-electron transducer in ISEs for the detection of Ca^{2+}, Pb^{2+}, moxifloxacin, and K^+, which achieved good potential stability and sensitivity (close to a Nernstian response). Pretsch et al.[114] applied redox-active and lipophilic fullerene, which is a spherical form of carbon composed of carbon atoms arranged in a network of hexagonal and pentagonal rings,[115–118] for the preparation of an SC-ISE via self-assembly. They obtained Nernstian responses to K^+ with a linearity down to 10^{-5} M, without the O_2 interface alongside high stability.[114] However, in recent years, the application of fullerene in ISEs has significantly decreased due to the rapid development of state-of-the-art nanomaterials that exhibit higher performance and lower cost for potentiometric ion sensing.

Metal-based nanomaterials

Metal/metal oxide materials are widely utilized in SC-ISEs to enhance charge transport characteristics, mechanical stability, and electrical conductivity[119,120] due to their high conductivity and large surface area. Among various metal nanomaterials, silver nanoparticles have attracted considerable interest, since they exhibit anti-biofouling properties, a high electron transport rate and a large specific surface area. As a result, they could be applied as a component in the transducer layer of the solid contact[121] and as the surface modifier of the ion-selective membrane to provide the anti-biofouling feature.[122] Silver nanoparticles have a prominent antibacterial property to eliminate microorganisms, making them promising for detecting ions in biological samples under harsh environments. Another attractive metal nanomaterial used in SC-ISEs is gold nanoparticles,[23,123] first proposed by Michalska and co-workers.[124] It was found that gold nanoparticles with a longer alkyl chain ligand (Au@C8) improved the selectivity of the SC-ISE. Subsequent reports also highlighted that gold nanoclusters served as effective transducers in the design of high-performance SC-ISEs.[29,125] Gold nanomaterials have been successfully employed to immobilize ion recognition components

such as ionophores,[126] bio-receptors,[127] and aptamers[128] to increase selectivity. Due to the excellent electrical properties, biocompatibility, biochemical activity, and multi-functionality, gold nanoparticles find wide applications in potentiometric biosensors.[129,130] Zhang and co-workers[129] developed a multi-calibrated urea potential sensing array with three main parts, namely, a urea electrode group, a reference channel, and a pH electrode group. The pH electrode group contains a calibration channel, and the basic potential of sensing channels could be adjusted using the respective calibration channels. The urea electrode group consists of a sensing channel and Au@urease nanoparticles were applied as the sensing material to increase the stability of the sensor. The pH electrode group could measure pH values and calibrate the response slope of the urea electrode cluster using the calibration coefficient. Fig. 5A (a) illustrates the preparation process for the multicalibration urea potential detection array (b) and Au@urease nanoparticles. In addition, bimetallic nanoparticles composed of two metals such as Au–Ag and Ni–Pt exhibited unique properties as electrochemical catalysts due to the high surface area, synergetic effects, and high catalytic activity.[30,131–133] Transition metal nanoparticles were also developed as the sensing membrane or solid contact to improve the potential stability, reproducibility, response time, and lifetime due to large surface areas and multiple oxidation states.[134–136]

Nanoporous metal materials have attracted considerable interest for the development of SC-ISEs due to their numerous interconnected nano-sized cavities that can provide a large area for ion interaction and adsorption.[137–139] For example, nanoporous gold film and platinum oxide were used widely as the solid contact in ISEs, which demonstrated high potential stability with a short response time.[140–142] The impact of different types of metal oxide nanoparticles as the solid contact, including zinc oxides, iron oxides, and copper oxides, on the sensing performance of ISEs for K^+ detection was studied by Wardak et al.[120] It was found that the integration of metal oxide nanoparticles into the electrode enhanced its performance, particularly in terms of electrical parameters and potential stability; this could be attributed to excellent electrochemical activity and a high surface-to-volume ratio. In addition, the best performance was achieved by using zinc oxide nanoparticles, with a low LOD (3.66×10^{-6} mol L^{-1}), a fast response time (4–6 s), and sustained functionality over 5 months. The superior characteristics of electrodes utilizing zinc oxide nanoparticles might be attributed to greater homogeneity. A graphical depiction of the modification of a glassy carbon electrode (GCE) with metal oxide nanoparticles and a membrane, alongside a SEM image of the zinc oxide nanoparticles and calibration curve for the zinc oxide electrode, is shown in Fig. 5B.

Recently, MOFs consisting of metal ions or clusters coordinated with organic ligands to form an ultra-high porous structure[143,144] have been highly favored for the development of SC-ISEs. Mirica et al.[145] proposed an SC-ISE using a conductive MOF as the ion-to-electron transducer. This electrode was prepared by modifying a GCE with MOFs through drop
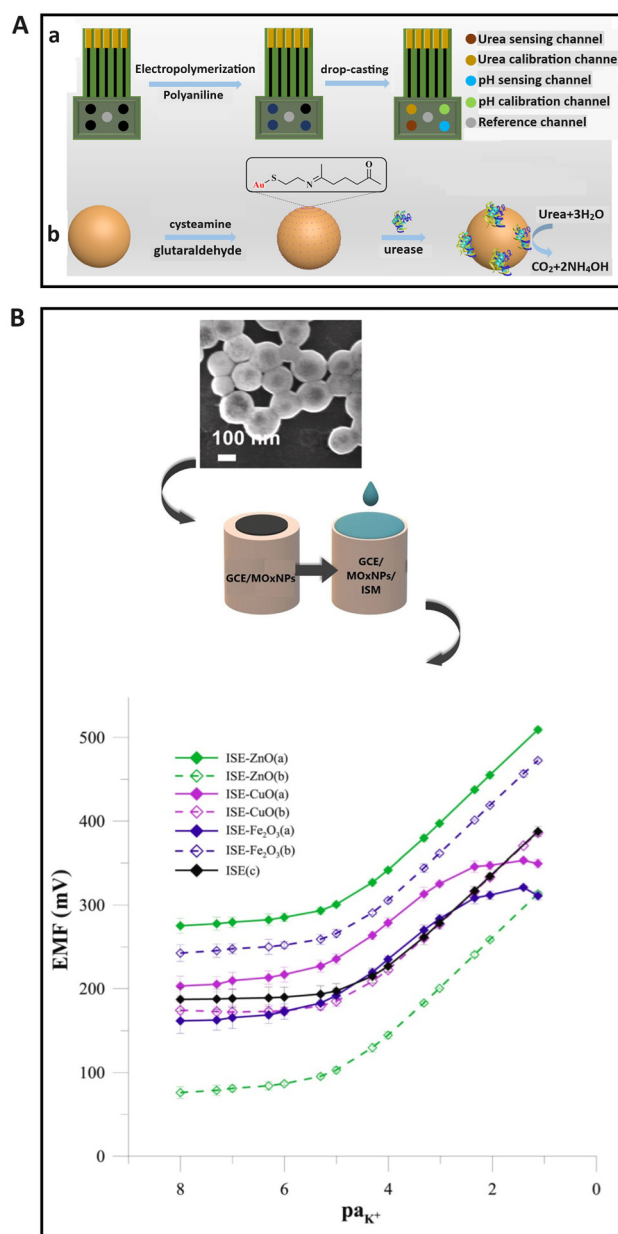

Fig. 5 (A) A graphical depiction of the preparation process of (a) a sensing array of multicalibrated urea potential, and (b) Au@urease nanoparticles.[129] Copyright 2022, ACS publications. (B) Schematic illustration of the modification process for a GCE with metal oxide nanoparticles and membrane, alongside a SEM image of zinc oxide nanoparticles and calibration curves of unmodified and different metal oxide nanoparticle-based-ISEs (ZnO, CuO, and Fe_2O_3) in KNO_3 solution over the concentration range of 1×10^{-8}–1×10^{-1} mol L^{-1} after two months of measurements.[120] Copyright 2022, Elsevier.

casting, followed by modification of a K^+ or NO^{3-} selective membrane. The ISE showed a very good performance close to Nernstian behavior (54.1–58.2 mV s^{-1}) with a satisfactory signal stability (15 ± 1 μV s^{-1}) and a wide dynamic range spanning from millimolar to nanomolar concentrations for the detection of K^+ and NO_3^-. Recently, Asadnia and co-workers[146] investigated the impact of using Ni-HAB MOFs as the ion-to-

electron transducer in an SC-ISE for the detection of Li$^+$. It was found that the capacitance of the sensor was raised by increasing the thickness of MOFs, which led to long-term stability with a 1.15×10^{-6} mV h^{-1} drift over 12 h. In principle, the high capacitance of the ion-to-electron transducer layer helps to prevent polarization due to a minimal electrical current, resulting in a quicker and more stable response.[146] Although the low electrical conductivity of MOFs may limit their application in SC-ISEs, their high proton conductivity and compatibility with highly conductive materials enable the development of effective nanocomposite-based solid contacts. Moreover, their interconnected and tunable pore sizes make them promising candidates as solid contacts or ionophores for the preparation of SC-ISEs.[147–151]

Recently, Fouad et al.[152] synthesized Mullite nanoceramics using the sol–gel method; these were used as ionophores in carbon paste of ISEs for the detection of Cd^{2+}. The mechanism of action was based on ions binding to the surface of the electrode containing Mullite nanoparticles. Since the mesoporous structure of Mullite significantly speeds up electron transfer processes, this work can be considered a good example of the high potential of porous nanomaterials for ionophore preparation. Chen, Ge et al.[128] developed a portable Ca^{2+} ISE by using phenylboronic acid-functionalized nanometer-sized CaCO$_3$ particles as the recognition and signal elements for monitoring carcinoembryonic antigen glycoprotein. In order to maintain the bioactivity, the carcinoembryonic antigen aptamers were immobilized on the Au substrate. In addition, phenylboronic acid-functionalized nanometer-sized CaCO$_3$ enhanced the storage stability by facilitating the retention of organoboron-conjugated nanomaterials and aptamers on the Au substrate.

Polymer-based nanomaterials

Nanosized conductive polymers used as the ion-to-electron transducer layer have broadened the applications of ISEs by improving their sensing performance.[153,154] For example, Yehia et al.[155] developed an SC-ISE for flunitrazepam determination in beverages using poly(3,4-ethylenedioxythiophene) nanoparticles, which generated a conductive and hydrophobic polymer layer on the electrode surface to achieve good selectivity and a low detection limit. Zhang and co-workers[156] employed poly(3-octylthiophene-2,5-diyl) and carbon black as the transducer in an SC-ISE to improve the sensitivity for the detection of K$^+$. Various polymeric nanofibers such as poly(3,4-ethylenedioxythiophene) have been used in SC-ISEs as a component of the solid contact for the detection of Pb^{2+}.[157] However, the impact of pH on the sensing performance of this material, which is one of the important parameters for practical applications, was not reported in this work. Shaban et al.[158] prepared an m-cresol nanopolymer-based electrode for the potentiometric sensing of Pb^{2+}, which showed a good Nernstian response, low detection limit (1.0×10^{-7} M), high selectivity and good stability under ambient conditions.

Michalska et al.[159] reported modified polyvinylidene fluoride nanofibers with bis(2-ethylhexyl)sebacate as a receptor for

K$^+$ detection. The thickness of the ion-selective layer was below 10 nm, but the electrolyte diffusion coefficient for the nanofiber phase was estimated to be 10^{-10} cm^2 s^{-1}, which was considerably lower than the values typically associated with ion transport through traditional poly vinyl chloride (PVC)-based membranes. This could be related to the effect of air trapped in the pores of the nanofiber mats, which hinders the penetration of this phase by water, indicating that the rate limiting step in this process is filling the nanofiber mat pores with electrolyte.

Among various types of polymer nanomaterials, polyaniline (PANI) is more favourable for the design of high-performance ISEs owing to its high conductivity, environmental stability, low cost, versatile production methods along with simple setup.[160–163] In addition, it was found that the morphology of PANI had a significant effect on the sensing performance of SC-ISEs.[164,165] For instance, 3D PANI nanowire arrays (NWA) used as the ion-to-electron transducer layer offered a better performance, including faster response (approximately 1 s) and lower detection limit (2.5×10^{-8} M) for the selective detection of Pb^{2+}, than PANI micro-/nanowire networks (MNWN) and micro-/nanosheets (MNS).[166] This performance can be attributed to the high double-layer capacitance and enhanced diffusion of Pb^{2+} through the transducer layer due to the open structure of nanowire arrays, as shown in Fig. 6A and B.[166]
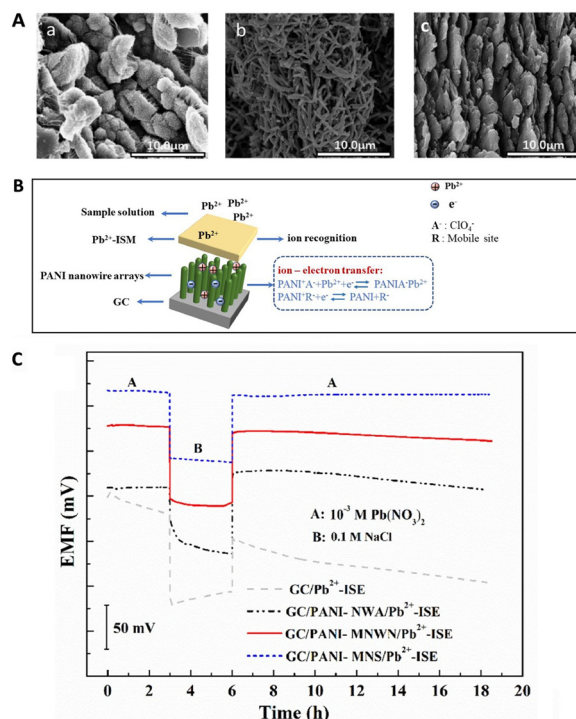

Fig. 6 (A) SEM images of PANI-NWA (a), PANI-MNWN (b), and PANI-MNS (c) deposited on a glassy carbon electrode by direct electro-deposition. (B) Sensing mechanism for a NWA-based ISE. (C) Potential curves of different Pb^{2+}-ISEs in 10^{-3} M Pb(NO$_3$)$_2$ for 3 h, 0.1 M NaCl for 3 h, and then 10^{-3} M Pb(NO$_3$)$_2$ again for 12.5 h.[166] Copyright 2021, Elsevier.

Fig. 6C compares the stability of the potential response of the various Pb^{2+} ISEs, indicating that the potential drift significantly decreased by introducing PANI micro-/nanomaterials. Furthermore, the PANI-NWA can inhibit the formation of the water layer most efficiently due to its hydrophobic character, as observed in the water contact angle measurement. Additionally, PANI nanoparticles and nanofibers were utilized as the solid contact of ISEs, which achieved fast and stable Nernstian responses for the sensing of flucarbazone herbicide, Cr^{3+}, Cr^{6+}, NH_4^+, NO_3^-, alcaftadine, and cephalosporin.[160,167–170] In general, nanostructured polymers have good flexibility and elasticity, besides the typical properties of nanomaterials, making them promising candidates for the development of wearable and stretchable SC-ISEs in real-time analysis.

Nanocomposites

In recent years, the development of nanocomposite materials with a synergetic effect to maximize the sensing performance of SC-ISEs has attracted increasing interest. For example, the CNT–polymer nanocomposite is a typical material used in SC-ISEs to increase mechanical stability, alongside flexibility and conductivity.[171,172] Paczosa-Bator et al.[173] reported the construction of super-hydrophobic nanocomposite layers consisting of MWCNTs, carbon black, poly(3-octylthiophene-2,5-diyl), and hydrous iridium dioxide for K^+ determination. Michalska and co-workers[174] developed the MWCNT–poly(3-octylthiophene-2,5-diyl) (POT) nanocomposite as a transducer layer to promote the sensing performance of the electrode for the detection of K^+. The MWCNTs were well dispersed by POT, which eliminated the use of a surfactant as a stabilizer. Additionally, the undesired partitioning of POT to the membrane phase was prevented, which led to the high potential stability of the potentiometric sensor.

Ni_2O_3/RGO nanocomposites exhibit high electrochemical performances as a transducer element for the sensing of NO_3^- due to the synergistic effect between RGO and Ni_2O_3 nanostructures.[175] Generally, the combination and interaction of the components play a major role in nanochannels, leading to an attractive sensing performance, such as good selectivity and long-term stability.[30,176,177] For example, graphene/PVC and gold–CNT–gold nanocomposites were developed as a transducer material for the detection of tenofovir disoproxil fumarate[178] and Na^+,[179] respectively. Many studies reported that CNTs were promising components in nanocomposites for enhancing the analytical performance of the ISEs due to their high aspect ratios and high functionalization ability.[174,180–182] Recently, Hernández-Varela et al.[181] developed an ISE based on cellulose/MWCNTs as the transducer for detecting K^+. The homogeneous dispersion of cellulose aerogel (CA) and CNT ink increased the electrical and conductive behaviour of the ISE, and the resulting solid network exhibited good mechanical properties. The ISE shows a near Nernstian response (52.04 ± 0.26 mV) with a linear range from 10^{-4} to 10^{-1} M, while the LOD is 8.49×10^{-3} M, which is higher than that of many other K^+ sensors. Additionally, a detailed evaluation of important parameters such as long-term potential stability and capaci-

tance was not provided. Fig. 7A shows a scheme of the potentiometric cell and photos of the prepared K^+ ISE. The potentiometric response, the calibration plot, and preparation steps for the cellulose–CNT nanocomposite aerogel are shown in Fig. 7B, C and D, respectively. While using specific types of nanomaterials like an aerogel could offer potential improvements in ISEs, the LOD of the prepared sensor was 8.49×10^{-3},
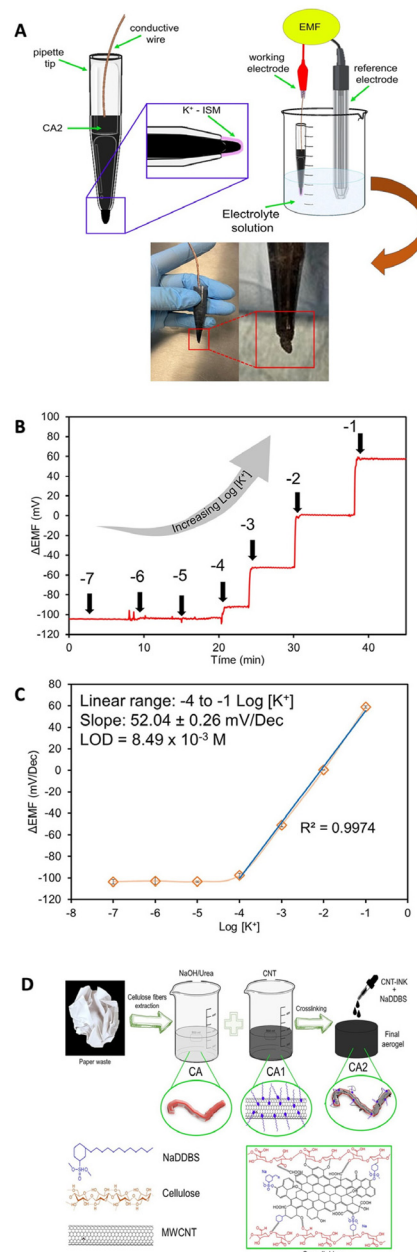
Fig. 7 (A) Graphical representation of an ISE based on cellulose/MWCNT nanocomposites as a component of a potentiometric cell with accompanying photographs, (B) the potentiometric response time trace, (C) calibration curve, and (D) graphical depiction of the preparation steps for the nanocomposite, including the preparation of CA, addition of CNTs (CA1), and incorporation of CNTs and NaDDBS ink to prepare the functionalized aerogel.[181] Copyright 2023, Wiley.

which was higher than those reported in similar studies. Also, the authors did not provide information on important parameters such as long-term potential stability and capacitance.

The application of MOF-based nanocomposites as a solid contact has been on the rise in recent years, owing to their high electrical conductivity, charge mobility, and surface area.[32,183,184] For the same reasons, MOFs are also widely used as a component of carbon paste in ISEs to improve their sensing performance. For example, 2D Cu-MOF : tricresyl phosphate (TCP) : graphite mixture in a ratio of 2.67 : 30.54 : 66.79 (wt/wt%) was prepared in the form of carbon paste for the detection of Cu^2, where graphite, 2D Cu-MOF, and TCP acted as the matrix, the electroactive material, and the plasticizer, respectively.[185] The results displayed Nernstian behavior with a fast response time (3–5 s) and pH independency in real samples, including red and mate tea, sesame seeds, human hair, and tap water (non-drinking water).

In recent years, the development of flexible and miniature SC-ISEs has been highly desirable to meet the increasing demand for wearable devices. Zhang et al.[32] synthesized a nickel triphenylene-fused metal catecholate (NiCAT) nanowire array on carbon nanotube fibers (CNTF) for the development of a wearable SC-ISE for sweat sensing. Fig. 8A shows photographs of the attachment of the wearable sensor to the forehead, construction details and a schematic diagram of the NiCAT@CNTF based ISE and RE in an electrochemical cell, as well as SEM images of the NiCAT@CNTF material, indicating that MOF nanowires aligned the carbon nanotube fibers as the transducer. This sensor exhibited a stable potential response alongside a good calibration curve and real-time sweat monitoring, as shown in Fig. 8A. The extremely high double-layer capacitance (34.39 mF cm^{-2}) of the solid contact transducer can be attributed to the small contact impedance and ordered porous structure of the nanomaterials. In addition, biomimetic zirconium MOF/polyvinylidene fluoride (PVDF) was used as the solid contact for the detection of Cl^-.[186] The different components of the miniaturized MOF-integrated potentiometric sensor, alongside the sensor setup and portable potentiostat are depicted in Fig. 8B. The miniaturized wireless electrochemical sensing system demonstrates the high portability of the sensor, making it suitable for real-time, on-site and remote detection of Cl^-.

Core–shell nanomaterials exhibit unique characteristics by combining the properties of the inner and outer parts when applied to ISEs.[187,188] Kaushal and Singh et al.[189] developed a highly selective core–shell nanocomposite electrode based on boron doped graphene oxide–aluminium fumarate metal–organic framework (BGO/AlFu MOF core–shell) for the detection of Br^-, showing a close to Nernstian response at low con-
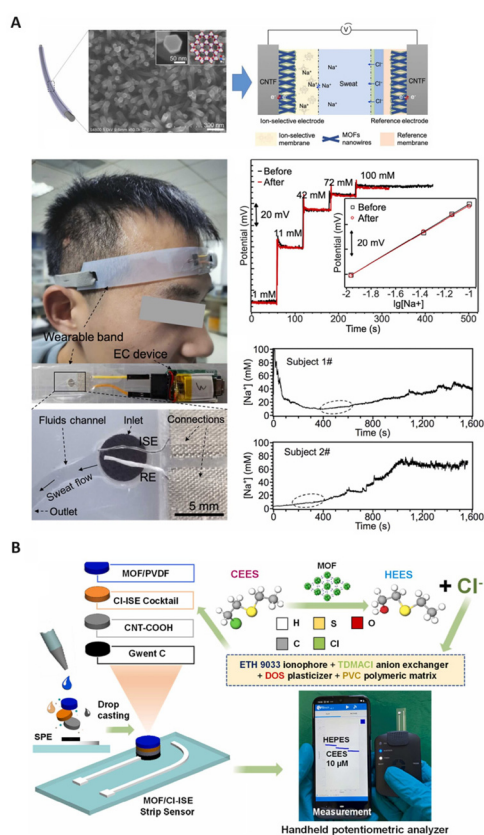
Fig. 8 (A) SEM images of the NiCAT nanowire array, along with a photograph of a flexible and wearable ISE based on MOF nanowires aligned on carbon nanotube fibers (CNTF), including their position in the sensor, potential response, calibration curves, and typical real-time sweat monitoring.[32] Copyright 2022, Elsevier. (B) Graphical representation of the miniaturized MOF-integrated solid contact, the sensor components, and its sulfur mustard detection mechanism using a miniaturized portable potentiostat for simulant analysis on a Bluetooth-interfaced smartphone.[186] Copyright 2023, Elsevier.

Fig. 9 (A) Overview of a wireless all-in-one sodium sensor with a solid-state ISE (SS-ISE) and a reference electrode (RF), attached to different substrates. (B) Graphical depiction of the SS-ISE and RF, and the production steps for the SS-ISE.[179] Copyright 2021, Elsevier.

Table 1 The sensing performance of various nanomaterials in SC-ISEs

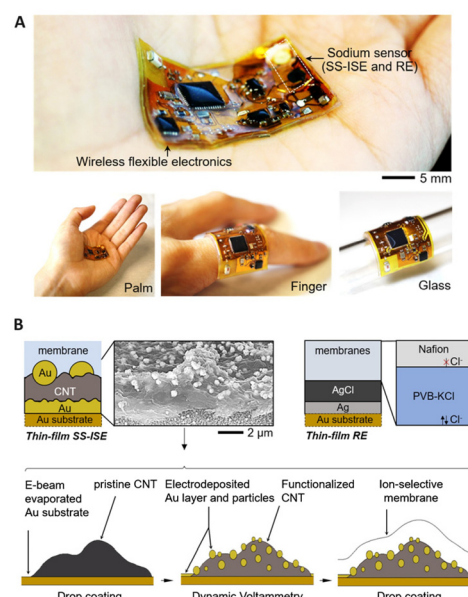| Nanomaterials & nanocomposites	Component	Transduction mechanism	Analyte	Sensitivity (mV per decade)	$E^{\ominus\,a}$ (mV)	Response time (s)	Linear range (M)	LOD (M)	Capacitance (μF)	Potential drift (μV h⁻¹)	Ref.
Carbon nanofibers/nickel–cobalt nanoparticles/CNT layer	Solid contact transducer	Double-layer	K^+	59.39 ± 0.80	413.7 ± 0.9	—	10^{-6}–10^{-1}	$10^{-6.3}$	330	20	53
Single-walled carbon nanohorns	Solid contact transducer	Double-layer	Ca^{2+}	29.69	—	4	10^{-6}–10^{-2}	$10^{-6.1}$	23.26	120	110
Graphene	Solid contact transducer	Double-layer	K^+	53.53	± 0.7	8	10^{-4}–10^{-1}	$10^{-4.28}$	—	2844	202
MOF (Cu_3(HHTP)$_2$)	Solid contact transducer	Redox	Cu^{2+}	29.5 ± 0.3	173.8 ± 3.5	10	10^{-2}–10^{-4}	$10^{-4.5}$	600	—	183
MWCNTs/Cu(II)-MOF	Solid contact transducer	—	Orphenadrine citrate	60.05 ± 0.16	—	8 ± 1.3	10^{-8}–10^{-2}	4×10^{-9}	—	—	203
MOF (NH$_2$-MIL-53(Fe))/PANI	Solid contact transducer	Redox	Epinastine hydrochloride	59.74 ± 1.61	—	5 ± 1	10^{-7}–10^{-2}	7.5×10^{-8}	—	50	150
Nano-cordierite (Mg$_2$Al$_4$Si$_5$O$_{18}$)	Ionophore	—	Sr^{2+}	29.1 ± 0.31	—	6	1.0×10^{-6}–1.0×10^{-2}	5.0×10^{-7}	—	—	204
Gold nanoparticle-reduced graphene oxide	Solid contact transducer	Double-layer	NH_4^+	56.94 (± 1.57)	—	<10	10^{-5}–10^{-2}	3.80×10^{-6}	123.5	8.1	199
Graphene/PANI	Solid contact transducer	Double-layer	Anti-COVID-19 drug remdesivir	55.39 ± 0.50	—	7 ± 1	10^{-7}–10^{-3}	1.00×10^{-7}	—	700	205
Ruthenium dioxide nanoparticle	Solid contact transducer	Double-layer	H^+	59	571 ± 2	5	10^{-12}–10^{-2}	—	1120	3204	206
Graphene/PVC	Solid contact transducer	—	Metoclopramide	59.90 ± 0.38	—	10	10^{-6}–10^{-2}	3×10^{-7}	—	2500	207
Graphene/PVC	Solid contact transducer	Double-layer	Tedizolid phosphate	-22.0 ± 0.2	—	7	10^{-6}–10^{-2}	7.9×10^{-7}	—	133	208
Mullite nano-ceramic in carbon paste	Ionophore	—	Carcinogenic Cd^{2+}	29.49 ± 0.24	—	6	1.0×10^{-8}–1.0×10^{-2}	1.0×10^{-8}	—	—	152
Ag nanoparticles/PANI	Solid contact transducer	Redox	Pb^{2+}	29.1 ± 0.3	—	<5	10^{-3}–10^{-9}	6.31×10^{-10}	40	90 360	121
Urease enzyme nanoparticles	Membrane	—	Urea	38	—	10–120	10^{-6}–80×10^{-5}	1×10^{-6}	—	—	209
Au nanoparticle/siloxene/graphene/poly(dimethylsiloxane)	Solid contact transducer	Double-layer	Na^+	60.13	421 ± 0.3	—	10^{-6}–$10^{-5.7}$	$5.6 \times 10^{-6.5}$	—	3	210
Au nanoparticle/siloxene/graphene/poly(dimethylsiloxane)	Solid contact transducer	Double-layer	K^+	59.4 ± 0.4	417 ± 0.5	—	$10^{-5.5}$	$8.1 \times 10^{-5.7}$	—	5	210
PANI	Solid contact transducer	Redox	Alcaftadine	58.8	—	5	1×10^{-6}–1×10^{-2}	6.3×10^{-7}	35.5	900	169
Graphene/carbon nanotube	Membrane	Double-layer	NH_4^+	59.6 ± 1.5	—	—	10^{-6}–10^{-1}	10^{-6}	—	—	211
Carbon black/soft elastomer	Solid contact transducer	—	Na^+	57	—	—	10^{-5}–1	4×10^{-6}	7.14	140	212
PANI nanofibers/MWCNTs	Solid contact transducer	Double-layer	Cl^-	-61.3	89.5 ± 1.8	<10	5×10^{-6}–1×10^{-1}	2.56×10^{-6}	7.16×10^3	30	180
Fe$_x$O$_y$ nanoparticles/LaF$_3$	Membrane	—	F^-	50.3–62.4	—	—	10^{-1}–3.98×10^{-7}	7.41×10^{-8}	—	—	119
Graphene nanocomposite	Solid contact transducer	—	Chlorhexidine	28.8 ± 0.2	—	15	10^{-6}–10^{-3}	4.76×10^{-7}	—	—	213
2D Ni-MOF nanosheets	Membrane cocktail	—	Ni^{2+}	29.5 ± 0.09	—	6	1.0×10^{-5}–1.0×10^{-1}	2.7×10^{-6}	—	—	214
Acylhydrazone-based MOF	Solid contact transducer	Redox	K^+	56.30	—	—	10^{-5}–10^{-1}	2.1×10^{-6}	—	320	215

Table 1 *(Contd.)*

Nanomaterials & nanocomposites	Component	Transduction mechanism	Analyte	Sensitivity (mV per decade)	$E^{\circ a}$ (mV)	Response time (s)	Linear range (M)	LOD (M)	Capacitance (µF)	Potential drift (µV h⁻¹)	Ref.
Poly(3-octylthiophene-2,5-diyl)/nanosized ruthenium dioxide	Solid contact transducer	Redox	K^+	58.64 ± 0.07	407 ± 1	—	10^{-1}–10^{-6}	$10^{-6.9}$	1170	28	216
Poly(3-octyl-thiophene)/molybdenum disulfide	Solid contact transducer	Redox	NO_3^-	64	—	—	1–1500 ppm NO_3–N	1.4 ppm	—	95	217
ZnO/RGO	Solid contact transducer	Redox	K^+	9.95 µA $(µM)^{-1}$ cm^{-2}	—	2	(100–500) 10^{-6}	956 × 10^{-6}	—	—	218
TiO²–CuO bimetallic/PANI	Solid contact transducer	—	Vildagliptin	60.04 ± 1.4	—	10 ± 1.3	1×10^{-2}–1×10^{-8}	4.5 × 10^{-9}	—	—	195
MWCNTs	Solid contact transducer	Double-layer	Fluoxetine	64.4 ± 0.2	—	<5 (for low concentrations)	6.0×10^{-7}–1.0×10^{-2}	2.0 × 10^{-7}	40.6 ± 2.1	88 560 ± 5040	55
SWCNTs/fullerene C_{60}/carbon nanoparticles	Solid contact transducer	Double-layer	Protonated procaine cations	58.9 ± 0.2	40.8 mB	7	5×10^{-7}–1×10^{-2}	$10^{-7.05}$	—	±330	190
Fullerene C_{60}–Nafion/SWCNT–fullerene C_{60}–PVC	Solid contact transducer	Double-layer	Procaine hydrochloride	58.0 ± 0.1	506.0 mB	≤5	1×10^{-7}–1×10^{-2}	$10^{-7.15}$	—	±140	190
SWCNTs	Solid contact transducer	Double-layer	Desvenlafaxine	57.2 ± 0.8	—	<8	—	2.0 × 10^{-6}	91.7 ± 3.4	10.6 ± 2.1	219
MWCNTs/PANI	Solid contact transducer	Double-layer	Erythromycin	54.0 ± 0.5	—	<10	4.6×10^{-6}–1.0×10^{-3}	9.6 ± 0.4 × 10^{-7}	324.7	11 160	220
Porous $NiCo_2S_4$ nanosheet	Solid contact transducer	Redox	Ca^{2+}	30.7 ± 0.3	0.3–0.7	—	1.0×10^{-9}–2.9×10^{-2}	1.6 × 10^{-7}	1800	1.9 ± 0.5	135
Polydopamine/Ag nanoparticles	Membrane	—	K^+	52.5 ± 1.8	—	4	1×10^{-4}–1×10^{-3}	$10^{-5.4}$	—	257.2	122
Au/CNT/Au	Solid contact transducer	—	Na^+	55.5 ± 0.3	—	—	10^{-3}–10^{0}	—	620.5	490	179
MOF nanowires/carbon nanotube fibers	Solid contact transducer	Double-layer	Na^+	58.69 ± 0.77	308.0 ± 3.1	—	10^{-5} to 10^{-1}	—	34 390 mF cm^{-2}	8.1 ± 4.1	32
Cellulose aerogel/CNTs/sodium dodecylbenzene sulfonate	Solid contact transducer	—	K^+	52.04 ± 0.26	—	—	10^{-4}–10^{-1}	8.49 × 10^{-3}	—	—	181
PANI/NWA	Solid contact transducer	Redox	Pb^{2+}	28–29	—	1	10^{-7}–10^{-3}	2.5 × 10^{-8}	27.2	132 120	166
Au@urease nanoparticles	Sensing material	—	Urea	−88.3 ± 1.5	—	—	5.0×10^{-3}–1.0	—	—	—	129
Mesoporous carbon	Solid contact transducer	Double-layer	Ag^+	55.6 ± 0.8	—	—	1.0×10^{-6}–1.0×10^{-3}	$10^{-6.8}$	—	115 200–86 400	93
RGO	Solid contact transducer	Double-layer	K^+	53.34	—	6	25×10^{-2}–6×10^{-5}	$10^{-4.24}$	—	7200	221
AuCu nanoparticles/MWCNTs	Solid contact transducer	Double-layer	Ca^{2+}	29.0	2.5	<10	10^{-6}–10^{-1}	6.03 × 10^{-7}	54	15 ± 3	30
AuCu nanoparticles/MWCNTs	Solid contact transducer	Double-layer	SO_4^{2-}	27.0	3.1	<10	10^{-5}–10^{-1}	8.91 × 10^{-6}	105	118 ± 16	30
Ag@AgCl nanomaterial/1-tetradecyl-3-methylimidazolium chloride	Solid contact transducer	Redox	Ca^{2+}	28.3	—	—	10^{-6}–10^{-2}	$10^{-6.5}$	75.2	47 880 ± 11 160	222
ZnO nanoparticles	Solid contact transducer	Double-layer	K^+	−56.07	350.18	4–6	1×10^{-5}–1×10^{-1}	3.66 × 10^{-6}	—	160	120
Ni–HAB MOFs	Solid contact transducer	Double-layer	Li^+	57.6	—	<1	—	9.94 × 10^{-7}	1652 (µF cm^{-2})	1.15 × 10^{-3}	146
Laser-induced graphene/PVC	Solid contact transducer	—	NO_3^-	−58.17 ± 4.21	—	—	$10^{-3.5}$–10^{-1}	6.01 ± 1.44 × 10^{-6}	95.24 ± 8.24	37 800 ± 3456	90

Table 1 (*Contd.*)

Nanomaterials & nanocomposites	Component	Transduction mechanism	Analyte	Sensitivity (mV per decade)	$E^{\circ\,a}$ (mV)	Response time (s)	Linear range (M)	LOD (M)	Capacitance (μF)	Potential drift (μV h⁻¹)	Ref.
Ordered mesoporous carbon	Solid contact transducer	Double-layer	K^+	63.5 ± 0.6	583 ± 9.1	8	$10^{-4.19}$–$10^{-0.21}$	5.4×10^{-6}	52.93	11 988 ± 2088	92
Boron doped graphene oxide–aluminium fumarate metal organic framework	Membrane	—	Br^-	54.53 ± 0.15	—	13	1×10^{-7}–1×10^{-1}	7.1×10^{-8}	—	—	189
Shelled hollow carbon nanospheres	Solid contact transducer	—	Ca^{2+}	28	—	—	10^{-5}–0.05	—	40	20	109
Molecularly imprinted polymers/PANI	Solid contact transducer	Double-layer	Flucarbazone anion	−45.5 ± 1.3	—	<5	10^{-2}–10^{-5}	5.8×10^{-6}	11.7 ± 0.7	41 760	167
Aliquat/PANI	Solid contact transducer	Double-layer	Flucarbazone anion	−56.3 ± 1.5	—	<5	10^{-2}–10^{-4}	8.5×10^{-6}	37.7 ± 1.2	141 480	167
Thiol-functionalized reduced graphene oxide	Solid contact transducer	—	K^+	60.0 ± 0.4	2.6 (SD)	<5	10^{-7}–10^{-1}	2.5×10^{-6}	12.43×10^{-6}	1.75	83
Thiol-functionalized reduced graphene oxide	Solid contact transducer	—	NO_3^-	−60.0 ± 0.5	4.8 (SD)	<5	10^{-7}–10^{-1}	4.0×10^{-6}	5.99×10^{-6}	8.79	83
Dibutylphthalate/MOF (MIL-53(Al))/PVC	Electroactive material	—	Imipramine hydrochloride	57.7	—	<5	1.0×10^{-7}–1.0×10^{-1}	5.0×10^{-8}	—	—	147

^{a} Standard potential, which is the potential recorded when the primary ion activity is set to 1.[23,223]

centrations (1×10^{-7}–1×10^{-1} M). The LOD and average slope of the calibration curve were 7.1×10^{-8} M and 54.53 ± 0.15 mV per decade change of concentration, respectively. Fullerene-based nanocomposites, owing to the high compatibility of fullerene with many materials, also serve as the solid contacts or membranes in SC-ISEs.[117,190,191] Over the past few years, a substantial number of studies on SC-ISEs focused on the exploration of novel nanocomposites with tailored structures and features as solid contact transducer layers or ion-selective membranes for the sensing of various ions.[135,167,192–195]

Wearable SC-ISEs have attracted considerable interest for the non-invasive and real-time monitoring of ions. Nanocomposites have been proposed as fascinating candidates for wearable sensors due to good biocompatibility and mechanical stability with high flexibility on the skin's surface, and good ion-to-electron transduction.[196–198] Recently, Doan and co-workers[199] developed NH_4^+-ISEs based on gold-nanoparticles–reduced graphene oxide as an ion-to-electron transducer. The prepared sensor exhibited high potential stability and a fast response time (<10 s) due to good hydrophobicity, conductivity, and an increased double-layer capacitance at the membrane/solid-contact interface (from 1.22 to 8.41 μF) due to the AuNP–RGO transducer layer. The linear range and detection limit were 10^{-5}–10^{-2} M and 3.80×10^{-6} M, respectively, without interference from light, carbon dioxide, oxygen, and redox species. The potentiometric response of the sensor in NH_4Cl solutions spanned the range from 10^{-7} to 10^{-2} M, with high potential stability and reversibility at low concentrations. However, since the composition of the nanocomposites in the solid contact was not characterized in detail, the mechanisms associated with the synergistic effect of the materials on the analytical performance were not well understood. A wearable all-in-one SC-ISE was developed for Na^+ detection based on nanocomposites of Au and CNTs (Fig. 9).[179] As shown in Fig. 9A, the Au/CNT/Au sensors and thin-layer circuits are fully encapsulated within a soft and biocompatible silicone elastomer membrane, which can be attached to different substrates. Fig. 9B indicates the preparation process for the nanocomposite transducer composed of CNTs and Au nanoparticles, along with a schematic and SEM images. The prepared nanocomposites exhibited an enhanced surface contact area and improved signal stability, leading to a sensitivity of 55.5 ± 0.3 mV per decade for Na^+. Although it was observed that the capacitance of the Au/CNT/Au electrode increased to 620.5 μF as compared to 75 μF for the Au/CNT electrode and 2.4 μF for the Au electrode, studies on the transduction mechanisms were not provided. The prepared thin electronic device with a thickness of 2 mm is promising for manufacturing miniaturized and wearable sensors. In addition, as reported by Bakker and Bobacka,[200,201] thin layers, as a class of nanomaterials, could also be used as membranes due to fast diffusion processes, despite some possible drawbacks such as low robustness, limited lifetime, and potential leakage of membrane components. Table 1 summarizes the sensing performance of various nanomaterial-based SC-ISEs developed over the past 5 years.

Conclusions and perspective

In this study, we provide a comprehensive review of the recent applications of various types of nanomaterials on SC-ISE sensing platforms. Although nanomaterials have been employed to enhance the properties of reference electrodes and ion-selective membranes such as mechanical strength and ionic selectivity, most of the reports focused on their utilization as an ion-to-electron transducer in SC-ISEs, which have been applied to detect various ions of environmental and biological interest. The unique nanostructures and high surface area of nanomaterials provide enhanced functionalities and interactions across interfaces of SC-ISEs; this makes them superior to the bulk materials in terms of sensing performance improvement. Among different types of nanomaterials such as carbon-, metal-, and polymer-based materials, nanocomposites with tailored compositions and structures have attracted increasing attention in recent years due to their good compatibility and high versatility, which can be attributed to synergetic effects in material combinations.

Although there has been a significant increase in the use of nanomaterials for the development of high-performance SC-ISEs over the past few years, the main challenges in this field include: (1) lack of a fundamental understanding of the structure–property–performance relationships for the rational design of nanomaterials in various SC-ISE applications; (2) poor reproducibility in sensor preparation because of the complex routes for nanomaterial preparation; (3) variations in sensing performance due to their high sensitivity to environmental conditions; (4) the potential toxicity of SC-ISE sensors that include heavy metals or engineered nanoparticles. Recent progress has indicated that nanomaterials are promising candidates for SC-ISE applications, particularly in the development of miniaturized, portable and wearable sensing devices for water quality and health monitoring, while the above-mentioned problems need to be addressed for their commercialisation for practical applications. This requires interdisciplinary efforts from various fields such as materials science, nanotechnology, sensor design and theory advancement. Furthermore, calibration-free ISEs, which are pre-calibrated when manufactured, offer fast measurements and user-friendly properties in environmental and clinical analyses. However, many of them have suffered from poor reproducibility and low stability due to potential variation and drift, resulting in low accuracy and reliability. Recently, advancements have been made in terms of improving the preparation methods and introducing innovative control measures. It is worth noting that the integration of novel materials into SC-ISE components is also a promising approach to address this challenge.

Conflicts of interest

The authors confirm that they have no conflict of interest.

Acknowledgements

References

1 G. Kaur, H. Kaur and S. K. Mittal, *Talanta Open*, 2022, **6**, 100158.
2 R. Ding, Y. H. Cheong, A. Ahamed and G. Lisak, *Anal Chem*, 2021, 1880–1888.
3 J. Baranwal, B. Barse, G. Gatto, G. Broncova and A. Kumar, *Chemosensors*, 2022, **10**, 363.
4 J. G. Manjunatha and C. M. Hussain, *Carbon Nanomaterials-Based Sensors: Emerging Research Trends in Devices and Applications*, 2022, p. 309.
5 A. Barhoum and Z. Altintas, *Fundamentals of Sensor Technology: Principles and Novel Designs*, Elsevier, 2023.
6 Y. Lyu, S. Gan, Y. Bao, L. Zhong, J. Xu, W. Wang, Z. Liu, Y. Ma, G. Yang and L. Niu, *Membranes*, 2020, **10**, 128.
7 A. K. Covington, *Ion Selective Electrode Method*, CRC press, 2018, vol. 1.
8 Ö. Isildak and O. Özbek, *Crit. Rev. Anal. Chem.*, 2021, **51**, 218–231.
9 H. Ryu, D. Thompson, Y. Huang, B. Li and Y. Lei, *Sens. Actuators Rep.*, 2020, **2**, 100022.
10 G. J. Mattos and E. Bakker, *Biosens. Bioelectron.: X*, 2023, **14**, 100351.
11 Y. Shao, Y. Ying and J. Ping, *Chem. Soc. Rev.*, 2020, **49**, 4405–4465.
12 J. Ding and W. Qin, *TrAC, Trends Anal. Chem.*, 2020, **124**, 115803.
13 Y. H. Cheong, L. Ge and G. Lisak, *Anal. Chim. Acta*, 2021, **1162**, 338304.
14 F. Trotta and A. Mele, *Nanosponges Synth. Appl.*, 2019, 1–26.
15 A. B. Asha and R. Narain, in *Polymer science and nanotechnology*, Elsevier, 2020, pp. 343–359.
16 F. S. Viteri and D. Diamond, *Analyst*, 1994, **119**, 749–758.
17 K. Motesharei and M. R. Ghadiri, *J. Am. Chem. Soc.*, 1997, **119**, 11306–11312.
18 N. E. Eltayeb and A. Khan, *J. Mater. Res. Technol.*, 2019, **8**, 2238–2246.
19 R. M. Kakhki, *Russ. J. Electrochem.*, 2013, **49**, 458–465.
20 M. Li, X. Zhou, X. Ma, L. Chen, D. Zhang, S. Xu, D. Duan, C. Chen, Q. Yuan and S. Liu, *Chem. Eng. J.*, 2021, **409**, 128164.
21 M.-R. Huang and X.-G. Li, *Prog. Mater. Sci.*, 2022, **125**, 100885.
22 Y. E. Chipangura, B. D. Spindler, P. Bühlmann and A. Stein, *Adv. Mater.*, 2023, 2309778.
23 C. R. Rousseau and P. Bühlmann, *TrAC, Trends Anal. Chem.*, 2021, **140**, 116277.

24 D. T. Jackson and P. N. Nelson, *J. Mol. Struct.*, 2019, **1182**, 241–259.

25 X. V. Chen and P. Bühlmann, *Curr. Opin. Electrochem.*, 2022, **32**, 100896.

26 R. W. Cattrall and H. Freiser, *Anal. Chem.*, 1971, **43**, 1905–1906.

27 N. H. Ho, D. L. Glasco and J. G. Bell, *ECS Sens. Plus*, 2022, **1**, 020601.

28 M. Cosio, M. Scampicchio and S. Benedetti, *Electronic noses and tongues*, Academic Press, Boston, MA, USA, 2012.

29 J. Xu, F. Jia, F. Li, Q. An, S. Gan, Q. Zhang, A. Ivaska and L. Niu, *Electrochim. Acta*, 2016, **222**, 1007–1012.

30 Y. Liu, Y. Liu, R. Yan, Y. Gao and P. Wang, *Electrochim. Acta*, 2020, **331**, 135370.

31 J. Bobacka, *Electroanalysis*, 2006, **18**, 7–18.

32 S. Wang, M. Liu, Y. Shi, X. Yang, L. Li, Q. Lu, H. Zheng, S. Feng, Y. Bai and T. Zhang, *Sens. Actuators, B*, 2022, **369**, 132290.

33 J. Bobacka, A. Ivaska and A. Lewenstam, *Chem. Rev.*, 2008, **108**, 329–351.

34 M. Fibbioli, W. E. Morf, M. Badertscher, N. F. de Rooij and E. Pretsch, *Electroanalysis*, 2000, **12**, 1286–1292.

35 E. Bakker and E. Pretsch, *TrAC, Trends Anal. Chem.*, 2005, **24**, 199–207.

36 A. E. F. Oliveira, A. C. Pereira, M. A. C. de Resende and L. F. Ferreira, *Talanta Open*, 2022, **5**, 100085.

37 T. Alizadeh and M. Rashedi, *Anal. Chim. Acta*, 2014, **843**, 7–17.

38 S. Hosseini, S. Madaeni, A. Heidari and A. Amirimehr, *Desalination*, 2012, **284**, 191–199.

39 S. O. Mirabootalebi and G. H. Akbari, *Int. J. Bio-Inorg. Hybrid Nanomater.*, 2017, **6**, 49–57.

40 E. Ahmadian, D. Janas, A. Eftekhari and N. Zare, *Chemosphere*, 2022, **302**, 134826.

41 S. A. Hassan, N. W. Nashat, M. R. Elghobashy, S. S. Abbas, A. A. Moustafa and A. M. Mahmoud, *Microchem. J.*, 2022, **178**, 107323.

42 S. Mirabootalebi, *Adv. Compos. Hybrid Mater.*, 2020, **3**, 336–343.

43 S. Papp, J. Kozma, T. Lindfors and R. E. Gyurcsányi, *Electroanalysis*, 2020, **32**, 867–873.

44 G. A. Crespo, D. Gugsa, S. Macho and F. X. Rius, *Anal. Bioanal. Chem.*, 2009, **395**, 2371–2376.

45 A. E.-G. E. Amr, A. H. Kamel, M. A. Al-Omar, E. A. Elsayed, A. Y. Sayed and H. S. Abd-Rabboh, *Anal. Methods*, 2021, **13**, 1495–1501.

46 M. Shaban and A. Galaly, *Sci. Rep.*, 2016, **6**, 25307.

47 S. SM Hassan, A. Galal Eldin, A. E.-G. E. Amr, M. A. Al-Omar, A. H. Kamel and N. M. Khalifa, *Sensors*, 2019, **19**, 3891.

48 R. S. Khoshnood, S. Akbari and T. M. Chenarbou, *J. Anal. Chem.*, 2022, **77**, 1057–1061.

49 S. S. Hassan, A. Galal Eldin, A. E.-G. E. Amr, M. A. Al-Omar and A. H. Kamel, *Sensors*, 2019, **19**, 2697.

50 S. S. Hassan, S. M. Abdelbasir, M. A. Fathy, A. E.-G. E. Amr, M. A. Al-Omar and A. H. Kamel, *Nanomaterials*, 2019, **9**, 1160.

51 S. İ. Aslaner and A. Demirel Özel, *Monatsh. Chem.*, 2022, **153**, 881–893.

52 Z. Barati, M. Masrournia, Z. Es'haghi, M. Jahani and J. Ebrahimi, *J. Chem. Technol. Biotechnol.*, 2022, **97**, 1234–1239.

53 B. Niemiec, M. Zambrzycki, R. Piech, C. Wardak and B. Paczosa-Bator, *Materials*, 2022, **15**, 4803.

54 H. S. Abd-Rabboh and A. H. Kamel, *Anal. Sci.*, 2020, **36**, 1359–1363.

55 H. S. Abd-Rabboh, H. M. Hashem, L. MS Al Shagri, A. E.-G. E. Amr, A. A. Almehizia, A. M. Naglah and A. H. Kamel, *Membranes*, 2022, **12**, 446.

56 L. M. Al Shagri, A. H. Kamel, H. S. Abd-Rabboh and M. A. Bajaber, *ACS Omega*, 2022, **7**, 32988–32995.

57 S. S. Hassan, A. H. Kamel and M. A. Fathy, *Anal. Chim. Acta*, 2022, **1227**, 340239.

58 G. A. Crespo, S. Macho and F. X. Rius, *Anal. Chem.*, 2008, **80**, 1316–1322.

59 P. Damala, E. Zdrachek and E. Bakker, *Electroanalysis*, 2023, **35**, e202200247.

60 D. Yuan, A. H. Anthis, M. Ghahraman Afshar, N. Pankratova, M. Cuartero, G. A. Crespo and E. Bakker, *Anal. Chem.*, 2015, **87**, 8640–8645.

61 E. Zdrachek and E. Bakker, *Microchim. Acta*, 2021, **188**, 1–10.

62 A. M. Zamarayeva, N. A. Yamamoto, A. Toor, M. E. Payne, C. Woods, V. I. Pister, Y. Khan, J. W. Evans and A. C. Arias, *APL Mater.*, 2020, **8**, 1–10.

63 S. Roy, M. David-Pur and Y. Hanein, *ACS Appl. Mater. Interfaces*, 2017, **9**, 35169–35177.

64 Y. Zhang, Z. Li, X. Guo, G. Liu and S. Zhang, *Sensors*, 2021, **21**, 350.

65 H. Afsharara, E. Asadian, B. Mostafiz, K. Banan, S. A. Bigdeli, D. Hatamabadi, A. Keshavarz, C. M. Hussain, R. Kecili and F. Ghorbani-Bidkorpeh, *TrAC, Trends Anal. Chem.*, 2023, 116949.

66 Y. Yu, M. T. Hoang, Y. Yang and H. Wang, *Carbon*, 2023, **205**, 270–293.

67 S. Mesarić and E. Dahmen, *Anal. Chim. Acta*, 1973, **64**, 431–438.

68 M. Javanbakht, M. R. Ganjali, P. Norouzi, A. Badiei, A. Hasheminasab and M. Abdouss, *Electroanalysis*, 2007, **19**, 1307–1314.

69 M. Javanbakht, A. Badiei, M. R. Ganjali, P. Norouzi, A. Hasheminasab and M. Abdouss, *Anal. Chim. Acta*, 2007, **601**, 172–182.

70 M. R. Ganjali, H. Khoshsafar, A. Shirzadmehr, M. Javanbakht and F. Faridbod, *Int. J. Electrochem. Sci.*, 2009, **4**, 435–443.

71 M. R. Ganjali, H. Khoshsafar, F. Faridbod, A. Shirzadmehr, M. Javanbakht and P. Norouzi, *Electroanalysis*, 2009, **21**, 2175–2178.

72 S. Ramezani, M. H. Mashhadizadeh, R. Jahani and M. Kamali, *Int. J. Environ. Anal. Chem.*, 2023, 1–24.

73 B. Singh and M. Dhiman, in *Advances in Aerogel Composites for Environmental Remediation*, Elsevier, 2021, pp. 217–243.

74 A. Razaq, F. Bibi, X. Zheng, R. Papadakis, S. H. M. Jafri and H. Li, *Materials*, 2022, **15**, 1012.

75 F. Li, J. Ye, M. Zhou, S. Gan, Q. Zhang, D. Han and L. Niu, *Analyst*, 2012, **137**, 618–623.

76 Z. A. Boeva and T. Lindfors, *Sens. Actuators, B*, 2016, **224**, 624–631.

77 M. Rutkowska, T. Lindfors, Z. Boeva and M. Strawski, *Sens. Actuators, B*, 2021, **337**, 129808.

78 R. Yan, S. Qiu, L. Tong and Y. Qian, *Chem. Speciation Bioavailability*, 2016, **28**, 72–77.

79 X. Cui, Y. Bao, T. Han, Z. Liu, Y. Ma and Z. Sun, *Talanta*, 2022, **245**, 123481.

80 A. Shirzadmehr, M. Rezaei, H. Bagheri and H. Khoshsafar, *Int. J. Environ. Anal. Chem.*, 2016, **96**, 929–944.

81 J. Li and W. Qin, *Anal. Chim. Acta*, 2019, **1068**, 11–17.

82 D. S. Kim, J.-M. Jeong, H. J. Park, Y. K. Kim, K. G. Lee and B. G. Choi, *Nano-Micro Lett.*, 2021, **13**, 1–14.

83 Y. Liu, Y. Liu, Z. Meng, Y. Qin, D. Jiang, K. Xi and P. Wang, *Talanta*, 2020, **208**, 120374.

84 J. Ping, Y. Wang, J. Wu and Y. Ying, *Electrochem. Commun.*, 2011, **13**, 1529–1532.

85 J. Ping, Y. Wang, Y. Ying and J. Wu, *Anal. Chem.*, 2012, **84**, 3473–3479.

86 S. Wang, L. Zhong, S. Gan, Y. Tang, S. Qiu, Y. Lyu, Y. Ma and L. Niu, *Electrochem. Commun.*, 2021, **129**, 107091.

87 R. R. Soares, R. G. Hjort, C. C. Pola, D. Jing, V. S. Cecon, J. C. Claussen and C. L. Gomes, *Microchim. Acta*, 2023, **190**, 43.

88 V. P. Wanjari, A. S. Reddy, S. P. Duttagupta and S. P. Singh, *Environ. Sci. Pollut. Res.*, 2023, **30**, 42643–42657.

89 E. R. Mamleyev, S. Heissler, A. Nefedov, P. G. Weidler, N. Nordin, V. V. Kudryashov, K. Länge, N. MacKinnon and S. Sharma, *npj Flexible Electron.*, 2019, **3**, 2.

90 R. G. Hjort, R. R. Soares, J. Li, D. Jing, L. Hartfiel, B. Chen, B. Van Belle, M. Soupir, E. Smith, E. McLamore, J. C. Claussen and C. L. Gomes, *Microchim. Acta*, 2022, **189**, 122.

91 R. t. Guo, X. Hu, X. Chen, Z. x. Bi, J. Wang and W. g. Pan, *Small*, 2023, **19**, 2207767.

92 Z. Jiang, X. Xi, S. Qiu, D. Wu, W. Tang, X. Guo, Y. Su and R. Liu, *J. Mater. Sci.*, 2019, **54**, 13674–13684.

93 T. Yin, T. Han, C. Li, W. Qin and J. Bobacka, *Anal. Chim. Acta*, 2020, **1101**, 50–57.

94 Y. Guo, T. Yin, J. Ding and W. Qin, *ACS Sens.*, 2023, **8**, 4198–4206.

95 C.-Z. Lai, M. A. Fierke, A. Stein and P. Bühlmann, *Anal. Chem.*, 2007, **79**, 4621–4626.

96 Y. Zhang, Y. Tang, R. Liang, L. Zhong, J. Xu, H. Lu, X. Xu, T. Han, Y. Bao, Y. Ma, S. Gan and L. Niu, *Membranes*, 2022, **12**, 903.

97 F. Arduini, S. Cinti, V. Mazzaracchio, V. Scognamiglio, A. Amine and D. Moscone, *Biosens. Bioelectron.*, 2020, **156**, 112033.

98 H. Aguilar-Bolados, M. Yazdani-Pedram and R. Verdejo, in *High-Performance Elastomeric Materials Reinforced by Nano-Carbons*, Elsevier, 2020, pp. 149–175.

99 B. Paczosa-Bator, *Talanta*, 2012, **93**, 424–427.

100 J. Kalisz, K. Wɛ©grzyn, K. Maksymiuk and A. Michalska, *Anal. Chem.*, 2022, **94**, 3436–3440.

101 B. Niemiec, R. Piech and B. Paczosa-Bator, *Molecules*, 2023, **28**, 4313.

102 M. Banks, F. Amirghasemi, E. Mitchell and M. P. Mousavi, *Sensors*, 2023, **23**, 1891.

103 Z. Zhang and I. Papautsky, *Electroanalysis*, 2023, **35**, e202100686.

104 V. Mazzaracchio, A. Serani, L. Fiore, D. Moscone and F. Arduini, *Electrochim. Acta*, 2021, **394**, 139050.

105 T. Ozer and C. S. Henry, *Electrochim. Acta*, 2022, **404**, 139762.

106 Z. Zhang and I. Papautsky, *Electroanalysis*, 2021, **33**, 2143–2151.

107 Z. Zhang, E. Boselli and I. Papautsky, *Chemosensors*, 2023, **11**, 48.

108 F. Amirghasemi, A. Soleimani, S. Bawarith, A. Tabassum, A. Morrel and M. P. Mousavi, *Bioengineering*, 2023, **10**, 655.

109 L. Zhao, Y. Jiang, H. Wei, Y. Jiang, W. Ma, W. Zheng, A.-M. Cao and L. Mao, *Anal. Chem.*, 2019, **91**, 4421–4428.

110 C. Jiang, Y. Yao, Y. Cai and J. Ping, *Sens. Actuators, B*, 2019, **283**, 284–289.

111 C. Wardak, K. Morawska, B. Paczosa-Bator and M. Grabarczyk, *Materials*, 2023, **16**, 1003.

112 N. S. Gadhari, J. V. Gholave, S. S. Patil, V. R. Patil and S. S. Upadhyay, *J. Electroanal. Chem.*, 2021, **882**, 114981.

113 L. Zhao, Y. Jiang, J. Hao, H. Wei, W. Zheng and L. Mao, *Sci. China: Chem.*, 2019, **62**, 1414–1420.

114 M. Fibbioli, K. Bandyopadhyay, S.-G. Liu, L. Echegoyen, O. Enger, F. Diederich, P. Bühlmann and E. Pretsch, *Chem. Commun.*, 2000, 339–340.

115 S. Masoomzadeh, T. Gholikhani, P. Aminroaia, A. Taghvimi and Y. Javadzadeh, *Comb. Chem. High Throughput Screening*, 2023, **26**, 2607–2613.

116 N. Tagmatarchis, *Advances in carbon nanomaterials: Science and applications*, CRC Press, 2012.

117 K. Y. Zhizhin, E. S. Turyshev, L. K. Shpigun, P. Y. Gorobtsov, N. P. Simonenko, T. L. Simonenko and N. T. Kuznetsov, *Int. J. Mol. Sci.*, 2024, **25**, 1124.

118 M. Fouskaki and N. Chaniotakis, *Analyst*, 2008, **133**, 1072–1075.

119 J. Radić, M. Bralić, M. Kolar, B. Genorio, A. Prkić and I. Mitar, *Molecules*, 2020, **25**, 5213.

120 K. Pietrzak, N. Krstulović, D. Blažeka, J. Car, S. Malinowski and C. Wardak, *Talanta*, 2022, **243**, 123335.

121 X. Zeng, W. Jiang, G. I. Waterhouse, X. Jiang, Z. Zhang and L. Yu, *Microchim. Acta*, 2021, **188**, 1–11.

122 L. Qi, T. Jiang, R. Liang and W. Qin, *Sens. Actuators, B*, 2021, **328**, 129014.

123 L. Zhang, Z. Wei and P. Liu, *PLoS One*, 2020, **15**, e0240173.

124 E. Jaworska, M. Wójcik, A. Kisiel, J. Mieczkowski and A. Michalska, *Talanta*, 2011, **85**, 1986–1989.

125 M. Zhou, S. Gan, B. Cai, F. Li, W. Ma, D. Han and L. Niu, *Anal. Chem.*, 2012, **84**, 3480–3483.

126 G. Jágerszki, Á. Takács, I. Bitter and R. E. Gyurcsányi, *Angew. Chem., Int. Ed.*, 2011, **7**, 1656–1659.

127 N. F. Silva, J. M. Magalhães, M. F. Barroso, T. Oliva-Teles, C. Freire and C. Delerue-Matos, *Talanta*, 2019, **194**, 134–142.

128 Y. Chen, B. Li, P. Lyu, H. F. Kwok, L. Ge and Q. Wu, *Anal. Bioanal. Chem.*, 2021, **413**, 1073–1080.

129 F. Wang, F. Zhang, Q. Wang and P. He, *Anal. Chem.*, 2022, **94**, 14434–14442.

130 C. Pérez-González, C. Salvo-Comino, F. Martín-Pedrosa, C. García-Cabezón and M. L. Rodríguez-Méndez, *Food Control*, 2023, **145**, 109425.

131 D. S. Idris and A. Roy, *Crystals*, 2023, **13**, 637.

132 J. D. Lee, J. B. Miller, A. V. Shneidman, L. Sun, J. F. Weaver, J. Aizenberg, J. Biener, J. A. Boscoboinik, A. C. Foucher and A. I. Frenkel, *Chem. Rev.*, 2022, **122**, 8758–8808.

133 N. Cao, J. Su, W. Luo and G. Cheng, *Int. J. Hydrogen Energy*, 2014, **39**, 9726–9734.

134 S. S. Hassan, M. A. Fathy, I. Moussa, M. Obaida and A. H. Kamel, *Sens. Actuators, B*, 2023, **380**, 133397.

135 Y. Li, J. Li and W. Qin, *Talanta*, 2023, **251**, 123797.

136 S. Drummer, T. Madzimbamuto and M. Chowdhury, *Materials*, 2021, **14**, 2700.

137 R. Mishra, J. Militky and M. Venkataraman, *Nanotechnology in Textiles*, 2019, pp. 311–353.

138 E. Kianfar and H. Sayadi, *Carbon Lett.*, 2022, **32**, 1645–1669.

139 E. M. Hussien and A. R. Derar, *SN Appl. Sci.*, 2019, **1**, 1–11.

140 T. Yin, D. Pan and W. Qin, *Anal. Chem.*, 2014, **86**, 11038–11044.

141 S. Park, H. Boo, Y. Kim, J.-H. Han, H. C. Kim and T. D. Chung, *Anal. Chem.*, 2005, **77**, 7695–7701.

142 J. Li, T. Yin and W. Qin, *Sens. Actuators, B*, 2017, **239**, 438–446.

143 H.-C. Zhou, J. R. Long and O. M. Yaghi, *Journal*, 2012, **112**, 673–674.

144 X. Zhang, Z. Chen, X. Liu, S. L. Hanna, X. Wang, R. Taheri-Ledari, A. Maleki, P. Li and O. K. Farha, *Chem. Soc. Rev.*, 2020, **49**, 7406–7427.

145 L. Mendecki and K. A. Mirica, *ACS Appl. Mater. Interfaces*, 2018, **10**, 19248–19257.

146 M. Abdollahzadeh, B. Bayatsarmadi, M. Vepsäläinen, A. Razmjou and M. Asadnia, *Sens. Actuators, B*, 2022, **350**, 130799.

147 Y. Subasi, G. S. Kanberoglu, F. Coldur, O. Cubuk and M. Zahmakiran, *Chem. Pap.*, 2022, **76**, 5105–5117.

148 R. G. Deghadi, A. S. Eliwa, A. E. Ali, W. M. Hosny and G. G. Mohamed, *Comments Inorg. Chem.*, 2021, **41**, 189–212.

149 N. F. Mahmoud, O. A. Fouad, A. E. Ali and G. G. Mohamed, *Ind. Eng. Chem. Res.*, 2021, **60**, 2374–2387.

150 N. A. Abdallah, *Int. J. Electrochem. Sci.*, 2023, **18**, 100140.

151 J. Liu, X. Zou, C. Liu, K. Cai, N. Zhao, W. Zheng and G. Zhu, *CrystEngComm*, 2016, **18**, 525–528.

152 O. A. Fouad, M. M. Wahsh, G. G. Mohamed, M. M. El Desssouky and M. R. Mostafa, *Microchem. J.*, 2023, **190**, 108623.

153 H. Liu, Z. Gu, Q. Zhao, S. Li, X. Ding, X. Xiao and G. Xiu, *Sens. Actuators, B*, 2022, **355**, 131102.

154 N. Coppedè, M. Giannetto, M. Villani, V. Lucchini, E. Battista, M. Careri and A. Zappettini, *Org. Electron.*, 2020, **78**, 105579.

155 M. A. Tantawy, E. H. Mohamed and A. M. Yehia, *Microchim. Acta*, 2021, **188**, 192.

156 H. Bao, J. Ye, X. Zhao and Y. Zhang, *Molecules*, 2023, **28**, 3242.

157 X. Zeng, Y. Liu, G. I. Waterhouse, X. Jiang, Z. Zhang and L. Yu, *Microchem. J.*, 2022, **177**, 107279.

158 E. S. M. Sayyah, M. Shaban and M. Rabia, *Adv. Polym. Technol.*, 2018, **37**, 1296–1304.

159 A. Baranowska-Korczyc, E. Jaworska, M. Strawski, B. Paterczyk, K. Maksymiuk and A. Michalska, *Analyst*, 2020, **145**, 5594–5602.

160 Y. Bao, J. Yan, J. Hu and J. Li, *Sens. Actuators, B*, 2023, **390**, 133997.

161 Y. Liu, X. Zeng, G. I. Waterhouse, X. Jiang, Z. Zhang and L. Yu, *J. Electroanal. Chem.*, 2023, **939**, 117472.

162 Y. Li, J. Wu, H. Zhang, J. Hu, S. Li and L. Li, *J. Mater. Sci.*, 2023, 1–11.

163 F. Kazemi, S. M. Naghib, Y. Zare and K. Y. Rhee, *Polym. Rev.*, 2021, **61**, 553–597.

164 H. J. N. P. D. Mello and M. Mulato, *Thin Solid Films*, 2018, **656**, 14–21.

165 S. Kulkarni, Y. Navale, S. Navale, N. Ramgir, A. Debnath, S. Gadkari, S. Gupta, D. Aswal and V. Patil, *Org. Electron.*, 2017, **45**, 65–73.

166 X. Zeng, Y. Liu, X. Jiang, G. I. Waterhouse, Z. Zhang and L. Yu, *Electrochim. Acta*, 2021, **384**, 138414.

167 A. H. Kamel, A. E.-G. E. Amr, N. S. Abdalla, M. El-Naggar, M. A. Al-Omar, H. M. Alkahtani and A. Y. Sayed, *Polymers*, 2019, **11**, 1796.

168 S. S. Hassan, A. H. Kamel, A. E.-G. E. Amr, M. Abdelwahab Fathy and M. A. Al-Omar, *Molecules*, 2020, **25**, 629.

169 O. G. Hussein, D. A. Ahmed, M. Abdelkawy, M. R. Rezk, A. M. Mahmoud and Y. Rostom, *RSC Adv.*, 2023, **13**, 7645–7655.

170 K. Pietrzak, C. Wardak and S. Malinowski, *Appl. Nanosci.*, 2021, **11**, 2823–2835.

171 C. Wardak, K. Pietrzak, K. Morawska and M. Grabarczyk, *Sensors*, 2023, **23**, 5839.

172 R. Nishimoto, Y. Sato, J. Wu, T. Saizaki, M. Kubo, M. Wang, H. Abe, I. Richard, T. Yoshinobu and F. Sorin, *Biosensors*, 2022, **12**, 559.

173 N. Lenar, R. Piech and B. Paczosa-Bator, *J. Electrochem. Soc.*, 2022, **169**, 127508.

174 D. Kałuża, E. Jaworska, M. Mazur, K. Maksymiuk and A. Michalska, *Anal. Chem.*, 2019, **91**, 9010–9017.

175 P. J. Sephra, C. Tharini, A. Sachdev and E. Manikandan, *J. Alloys Compd.*, 2024, 173414.

176 Y. Wu, T. Zhou, Y. Wang, Y. Qian, W. Chen, C. Zhu, B. Niu, X.-Y. Kong, Y. Zhao and X. Lin, *Nano Energy*, 2022, **92**, 106709.

177 C. S. Kushwaha, N. Abbas and S. K. Shukla, *Int. J. Biol. Macromol.*, 2022, **217**, 902–909.

178 M. A. Soliman, A. M. Mahmoud, E. S. Elzanfaly and L. E. A. Fattah, *Int. J. Electrochem. Sci.*, 2024, 100477.

179 H.-R. Lim, Y. Lee, K. A. Jones, Y.-T. Kwon, S. Kwon, M. Mahmood, S. M. Lee and W.-H. Yeo, *Sens. Actuators, B*, 2021, **331**, 129416.

180 K. Pietrzak, K. Morawska, S. Malinowski and C. Wardak, *Membranes*, 2022, **12**, 1150.

181 S. D. Gallegos-Cerda, J. J. Chanona-Pérez, J. D. Hernández-Varela and M. C. López, *J. Appl. Polym. Sci.*, 2023, **140**, e53891.

182 D. Mishra, A. Krause, H. S. Sahni and S. Chatterjee, *Diamond Relat. Mater.*, 2023, **137**, 110156.

183 L. Xu, S. Gan, L. Zhong, Z. Sun, Y. Tang, T. Han, K. Lin, C. Liao, D. He and Y. Ma, *J. Electroanal. Chem.*, 2022, **904**, 115923.

184 A. Sharma, A. Singh, V. Gupta, A. K. Sundramoorthy and S. Arya, *Trends Environ. Anal. Chem.*, 2023, e00200.

185 S. E. Elashery and H. Oh, *Anal. Chim. Acta*, 2021, **1181**, 338924.

186 S. S. Sandhu, A.-Y. Chang, P. A. I. Fernando, J. F. Morales, N. Tostado, J. Jernberg, L. C. Moores and J. Wang, *Sens. Actuators, B*, 2023, **375**, 132818.

187 Z. Wang, J. Qi, N. Yang, R. Yu and D. Wang, *Mater. Chem. Front.*, 2021, **5**, 1126–1139.

188 M. Asaduzzaman, X. Hui, M. S. Reza, G. B. Pradhan, S. H. Jeong, H. Song, M. A. Zahed, M. Sharifuzzaman and J. Y. Park, *Chem. Eng. J.*, 2023, **474**, 145836.

189 N. Kaur, J. Kaur, R. Badru, S. Kaushal and P. P. Singh, *J. Environ. Chem. Eng.*, 2020, **8**, 104375.

190 K. Y. Zhizhin, E. S. Turyshev, A. V. Kopytin, L. K. Shpigun, N. T. Kuznetsov, N. P. Simonenko, N. N. Zamyatina, M. S. Madraimov and G. I. Betenev, *Nanosyst.: Phys., Chem., Math.*, 2022, **13**, 688–697.

191 K. Pietrzak and C. Wardak, *Sens. Actuators, B*, 2021, **348**, 130720.

192 C. Wardak, K. Pietrzak and K. Morawska, *Appl. Nanosci.*, 2023, 1–12.

193 H. E. K. Ertürün, *Int. J. Electrochem. Sci.*, 2018, **13**, 9452–9465.

194 A. Paut, A. Prkić, I. Mitar, L. Guć, M. Marciuš, M. Vrankić, S. Krehula and L. Tomaško, *Sensors*, 2021, **22**, 297.

195 N. A. Abdallah, S. A. Ahmed, M. Almaghrabi and Y. M. Alahmadi, *Polymers*, 2023, **15**, 3991.

196 Y. M. Choi, H. Lim, H.-N. Lee, Y. M. Park, J.-S. Park and H.-J. Kim, *Biosensors*, 2020, **10**, 111.

197 M. Rostampour, D. J. Lawrence Jr., Z. Hamid, J. Darensbourg, P. Calvo-Marzal and K. Y. Chumbimuni-Torres, *Electroanalysis*, 2023, **35**, e202200121.

198 M. Şen, M. Oğuz and İ. Avcı, *Talanta*, 2024, **268**, 125341.

199 L. D. Nguyen, C. M. Dang and T. C. D. Doan, *Microchem. J.*, 2023, **190**, 108717.

200 T. Forrest, E. Zdrachek and E. Bakker, *Electroanalysis*, 2020, **32**, 799–804.

201 T. Han, A. V. Kalinichev, Z. Mousavi, K. N. Mikhelson and J. Bobacka, *Sens. Actuators, B*, 2022, **357**, 131416.

202 H. J. Park, J.-M. Jeong, J. H. Yoon, S. G. Son, Y. K. Kim, K. G. Lee and B. G. Choi, *J. Colloid Interface Sci.*, 2020, **560**, 817–824.

203 A. K. Kammoun, M. H. Abdelrahman, A. N. Khayyat, S. S. Elbaramawi, T. S. Ibrahim and N. A. Abdallah, *RSC Adv.*, 2023, **13**, 31017–31026.

204 N. Nasser, O. A. Fouad, M. M. Wahsh, M. Rizk, G. G. Mohamed and M. R. Mostafa, *Microchem. J.*, 2024, **199**, 109978.

205 N. F. El Azab and N. Ahmed, *Microchem. J.*, 2023, **190**, 108658.

206 N. Lenar, B. Paczosa-Bator and R. Piech, *Microchim. Acta*, 2019, **186**, 1–11.

207 S. S. El-Mosallamy, K. Ahmed, H. G. Daabees and W. Talaat, *Anal. Bioanal. Chem.*, 2020, **412**, 7505–7514.

208 A. M. Mahmoud, E. M. Moaaz, M. R. Rezk, E. M. Abdel-Moety and A. S. Fayed, *Electroanalysis*, 2023, **35**, e202200115.

209 M. Attri and S. Kumari, *Health*, 2024, **61**, 1–11.

210 X. Hui, M. Asaduzzaman, M. A. Zahed, S. Sharma, S. Jeong, H. Song, O. Faruk and J. Y. Park, *ACS Appl. Mater. Interfaces*, 2024, 9725–9735.

211 Y. Hua, M. Guan, L. Xia, Y. Chen, J. Mai, C. Zhao and C. Liao, *Biosensors*, 2023, **13**, 409.

212 H.-R. Lim, Y.-S. Kim, S. Kwon, M. Mahmood, Y.-T. Kwon, Y. Lee, S. M. Lee and W.-H. Yeo, *Sensors*, 2020, **20**, 3297.

213 N. Magdy, A. E. Sobaih, L. A. Hussein and A. M. Mahmoud, *Electroanalysis*, 2023, **35**, e202200119.

214 S. E. Elashery, N. F. Attia and H. Oh, *Anal. Chim. Acta*, 2022, **1197**, 339518.

215 P. Kościelniak, M. Dębosz, M. Wieczorek, J. Migdalski, M. Szufla, D. Matoga and J. Kochana, *Materials*, 2022, **15**, 579.

216 N. Lenar, B. Paczosa-Bator, R. Piech and A. Królicka, *Electrochim. Acta*, 2019, **322**, 134718.

217 M. A. Ali, X. Wang, Y. Chen, Y. Jiao, N. K. Mahal, S. Moru, M. J. Castellano, J. C. Schnable, P. S. Schnable and L. Dong, *ACS Appl. Mater. Interfaces*, 2019, **11**, 29195–29206.

218 C. Tharini, G. Iyappan, E. Manikandan and P. J. Sephra, *J. Mater. Sci.: Mater. Electron.*, 2023, **34**, 1474.

219 M. A. Bajaber and A. H. Kamel, *Polymers*, 2022, **14**, 4814.

220 A. A. Almehizia, A. M. Naglah, M. G. Alanazi, A. E.-G. E. Amr and A. H. Kamel, *RSC Adv.*, 2023, **13**, 35926–35936.

221 J. H. Yoon, H. J. Park, S. H. Park, K. G. Lee and B. G. Choi, *Carbon Lett.*, 2020, **30**, 73–80.

222 X. Zeng and W. Qin, *Talanta*, 2020, **209**, 120570.

223 P. Bühlmann and L. D. Chen, *Supramol. Chem.: Mol. Nanomater.*, 2012, **5**, 2539.